Technical University of Denmark

DTU

Optimization of Wind Turbine Operation by Use of Spinner Anemometer

Friis Pedersen, Troels; Sørensen, Niels N.; Vita, Luca; Enevoldsen, Peder

[Link back to DTU Orbit](#)

DTU Library
Technical Information Center of Denmark

DTU

Optimization of
Wind Turbine Operation
by Use of Spinner Anemometer

TF Pedersen, NN Sørensen, L Vita, P Enevoldsen

DTU

Author: TF Pedersen, NS Sørensen, Luca Vita, Peder Enevoldsen
Title: Optimization of Wind Turbine Operation by Use of Spinner Anemometer
Department: Wind Energy Department

Abstract:

A prototype spinner anemometer was developed from a standard scientific sonic anemometer with specially designed 1D sonic sensors. A model spinner anemometer was tested in wind tunnel with two sensor head configurations. The tests showed that the sonic sensors responded with a high influence factor on yaw errors, and that the sensors responded with sinusoidal behaviour to rotation of the spinner. The tests also revealed a significant "sensor head flow distortion effect" from the classic sensor heads. A full CFD analysis of the model spinner anemometer was made. The results showed that the calculations were almost insensitive to rotation and to wind speeds. For all flow angles up to 60° the azimuth variation was a pure sinus. The shape of the responses was found to be described with a simple function that over one revolution decreases the average value with a cosine to the flow angle and increases the amplitude with a sine to the flow angle. The relation can be used in a conversion algorithm for the spinner anemometer. Field measurements were made with the model spinner anemometer. The spinner anemometer measurements were compared to measurements from a standard 3D sonic anemometer. The results showed time traces of the two instruments that were very similar. The prototype spinner anemometer was mounted on a 3.6MW prototype wind turbine. Statistics of the yaw error showed an average of about 10°. The average flow inclination angle was about 1°. The spinner anemometer measurements were correlated with wind speed and wind direction from a free meteorology mast. The results showed that the gain factor of the yaw error was only 0.80, which indicates that the yaw error measurements were overestimated with the use of the K factors from the CFD analysis. The wind speed at the free mast ahead of the wind turbine was compared to the wind speed measured by the spinner anemometer while the wind turbine was yawing while idling or stopped. The results showed that average wind speeds compared well within about 1%. The power of the 3,6MW wind turbine was analysed for varying yaw error but though the yaw error varied with more than ±20° during the period it was not possible to verify an expected cosine squared variation of power with yaw angle. The reason is that there was not sufficient data at all relevant wind speeds at the different yaw angles.

Contents

Preface

This report concerns the assessment of a new wind measurement concept called a "spinner anemometer". The assessment regards its fundamental functionality and its ability to track yaw errors. In this respect the electric power were analyzed for dependency on the yaw error. The investigations were made in cooperation with Siemens, who provided a model spinner and an arrangement for testing the concept in the Velux wind tunnel and at the test site at Risø. Siemens also provided access for testing the spinner anemometer on a Siemens 3,6MW wind turbine.

Introduction

A central part of the control of a wind turbine concerns regulation of power and loads. Power shall be maximized while loads are minimized. Key parameters in controlling power and loads are relative wind direction and wind speed. The relative wind direction, or the yaw error, is an expression of how good the wind turbine is to find the accurate wind direction. Maximizing the power is almost the same as minimizing the yaw error because a larger projected rotor area will be exposed to the wind. Minimizing the yaw error is also a minimization of the dynamic loads, and thus minimization of fatigue. The wind speed is used for pitch control and regulation of power at higher wind speeds, and it is also being used for determination of the power performance of the wind turbine. Optimization of power and loads is therefore dependent on quite accurate measurements of the wind that the wind turbine experiences. This report considers in detail a new concept for measurement of wind speed and wind direction. The concept is called a spinner anemometer because the spinner of the wind turbine is used for the measurements. The concept has potentially a higher accuracy in yaw error measurements than existing nacelle anemometry methods because it is positioned before the rotor. It thus has a potential for improved optimisation of power and loads of horizontal axis wind turbines.

1 Existing Wind Measurement Concepts on Wind Turbines

Today "nacelle-anemometry" is used on all large wind turbines. Wind speed and wind direction is measured with sensors mounted on the top of the nacelle. Typically the sensors comprise cup anemometers and wind vanes or 2D sonic sensors. The sensors are also often doubled for redundancy, see Figure 1. Nacelle anemometry gives input to the control system about wind speed and relative wind direction. This information is used for yaw control, start up and shut down, as well as for power performance verification [1].

Figure 1 Arrangement of nacelle anemometry on top of the nacelle of modern wind turbines. The cup anemometers and wind vanes are mounted redundantly on support structures that may influence on the accuracy of the measurements of the instruments

Nacelle anemometry is hampered by the fact that the instruments are positioned behind the rotor where the wind is very complex. Nacelle anemometry is influenced by the mounting arrangement of the instruments, and of the wakes of the blade root vortices over the nacelle and of the flow distortion due to the nacelle. The complicated flow structure is demonstrated in Figure 2, showing the vorticity in the flow behind the rotor [2]. The flow effects behind the rotor cause high deviations in determination of the free wind speed and wind direction. This may again cause weak yawing characteristics of the wind turbine, which leads to losses in electric power and increase in loads. To some extent the flow distortion effects may be calibrated

by the use of a free mast, but for individual wind turbine positions in a wind farm there may be introduced additional deviations by local flow due to terrain effects and wakes of other wind turbines. These additional deviations may increase significantly with increasing complexity of terrain.

Compared to nacelle anemometry it is an advantage to mount the anemometry in front of the rotor, where the flow is undisturbed. Such arrangements were introduced in the 80's on smaller wind turbines, see Figure 3. The 55kW Bonus wind turbine used a rod sticking out from the centre of the hub and carried a cup anemometer and a wind vane. The rod was mounted at the back of the nacelle, and it was carried through the hollow shaft. At the hub it was supported with a bearing. The construction was technically complicated and expensive, and maintenance of the instruments was difficult.
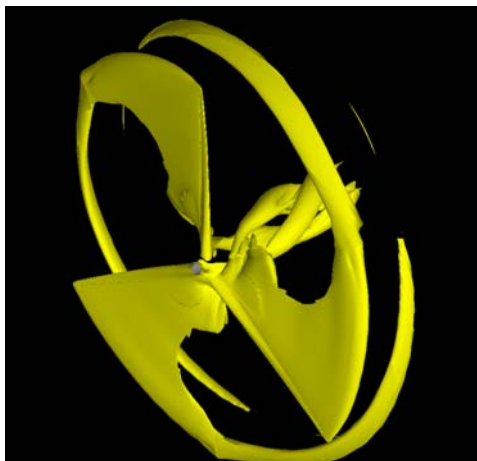

Figure 2 CFD calculation of vorticity around a wind turbine rotor [2]. The root vortices are seen to develop helical flow around the nacelle.

Figure 3 Arrangement of wind sensing instruments on a fixed arm extending from the spinner of a BOUNUS 55kW wind turbine

2 The Spinner Anemometer Concept

A newly developed alternative for measurement of wind speed and yaw error is the spinner anemometer. The concept of the spinner anemometer was presented for the first time at the EWEC 2007 conference [3]. Two other papers have been made on this concept [4,6], and a report on the CFD calculations [5]. A spinner anemometer is an anemometer that utilizes the flow over the spinner of the wind turbine to measure the wind speed, yaw error and flow inclination angle. The potentially improved measurement of the wind in front of the rotor by the use of a spinner anemometer, and the influence this may have on power and loads, is the content of this report. The spinner anemometer measures wind in front of and at the centre of the rotor where the wind flow is relatively undisturbed. The spinner itself does influence the flow around it, but in this case it is this influence that is actually part of the principle of the spinner anemometer. The induced wind speed at the centre line, due to induction of the blades, is significant. The blade roots influence also on the spinner anemometer, and this influence increases with the distance to the spinner nose. This means that the spinner do not fully represent the free wind. But otherwise, flow distortions on a spinner anemometer are rather uncomplicated as compared to the flow distortions experienced by nacelle anemometry.

2.1 Fundamental Principles

The shape of a spinner nose on most wind turbines is not much different from the shape of the nose of a pitot-tube or a pressure-sphere anemometer [7,8], though the size is somewhat larger. A pitot-tube nose is normally semi-spherical, and the measurement theory of the pitot-tube is based on the sphere. The sphere is also used for development of the theory of the spinner anemometer. One way to measure the wind speed could therefore be to measure the pressure differences from five holes in the spinner, similar to a five-hole pitot-tube. There are some disadvantages of this, though. One is the sensitivity of pressure tabs to rain and icing, and the other is the sensitivity to rotation.

A better measurement method is to measure directional wind speed in the flow over the spinner. A spinner is normally having a nice aerodynamic shape where the flow behaves in a well-defined manner without separation and thick boundary layers. For a spinner anemometer three directional wind speeds are measured above the boundary layer in three fixed and axially rotationally symmetric positions. The arrangement of wind speed sensors is in principle shown in figure 4. When the wind is coming directly along the shaft axis, all wind sensors will experience the same wind speed. When the wind angle of attack on the spinner changes, the three wind speeds at the sensors change. This change is used to determine the wind angle of attack on the spinner. The principle can be easily understood by considering figure 5 for a plane axial inflow (orange to the right in the figure) over a sphere that transforms into a cylinder. At the stagnation point at the nose centre the wind speed is zero on the spinner surface (blue). When moving from the stagnation point along the spinner surface, the wind speed increases. At about 50° on the spinner nose, the wind speed has reached a wind speed (orange) close to the free wind speed. Downwards from 50°, the wind speed increases further to a maximum (dark red), and then decreases again.

The wind measurement components of a spinner anemometer are three 1D sonic sensors having an inclined sensor path, an electronic conversion box and a wind turbine spinner, see figure 4. In principle, it is the same sensing components being used in a traditionally 3D sonic anemometer. Sonic anemometry is a conventional and robust measurement principle [10] without moving mechanical parts. Sonic anemometry also works well under icing conditions with internal heating of tubes and sensor heads [11]. The sonic sensors are mounted with the sensor paths in plane with the rotor axis and with the sonic paths tilted somewhat backwards to allow wind to come undisturbed into the sensor paths, avoiding sensor head shadow effects. In this way, the wind component on the sensors due to rotation is cancelled out, and only the wind along the axis direction is measured. The tilted-back configuration of the 1D sonic sensor also allows the sensor to be sufficiently narrow so that it can be mounted from the inside of the spinner through a hole in the mounting fitting on the spinner. This is a practical feature that makes mounting and maintenance easy. By converting the three wind measurements of the 1D sonic wind speed sensors to a representative spinner scalar wind, an angle of attack relative to the rotor axis and an azimuth angle on the spinner, all three wind components relative to a rotating spinner coordinate system are determined. In order to convert the wind components from the spinner coordinate system to a non-rotating stationary coordinate system, fixed with the nacelle, an accurate azimuth angle, or rotor position, also has to be measured, and used in the conversion.
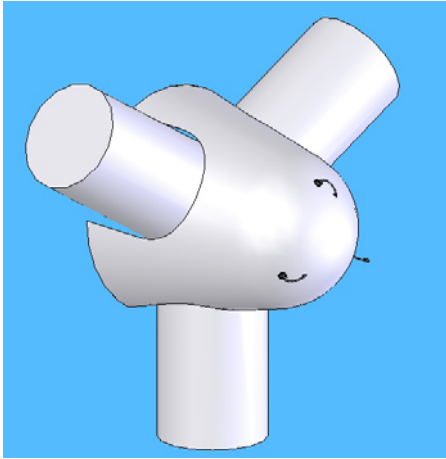
Figure 4 The concept of a spinner anemometer with three 1D sonic sensors mounted on the front part of the spinner. The spinner is in this figure shown with a spherical nose with a transition to a conical part.
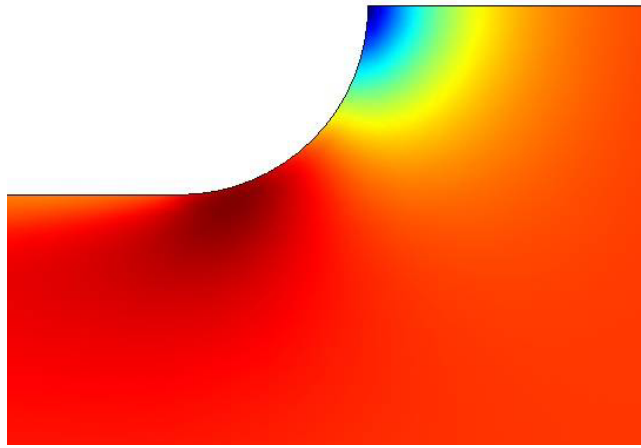

Figure 5 Wind speed contours around a rotational symmetric spinner with a spherical nose but without rotation (wind from the right). Notice the zero wind speed at the stagnation point of the nose (dark blue), the "free" wind speed (orange) at about 50° position over the surface of the spherical part, and the maximum speed (dark red) close to the transition from spherical to cylindrical part (COMSOL simulation).

The spinner anemometer concept comprises some other features. The rotation of the spinner anemometer has the natural consequence that the average values of each sonic sensor, over time, must be the same. This feature can be used to make an "internal" calibration of the sensors against each other. This internal calibration will compensate for inaccuracies of the spinner shape, off-axis mounting, and of inaccuracies of wind sensor mountings. The internal calibration assures that instantaneous wind measurements can be made very accurate. Another consequence of the rotation of the spinner anemometer is that each wind sensor can be used separately to give average wind speed and wind direction values by averaging over time. This makes the system accurate, redundant and very robust.

2.2 Spinner Anemometer Sensing Components

The spinner anemometers being used in the project were based on standard sonic sensor technology. A standard USA-1 scientific 3D sonic anemometer from Metek GmbH was the basis. The 3D sonic sensor arrangement was substituted with three specially designed separate 1D sonic sensors. Each sonic sensor was designed with a theoretical model based on potential flow over a sphere. A sensor with a path inclination angle of 23° to the sensor foot was found appropriate. Two prototype sensor types were produced with Metek sonic sensor heads. One type with classic sensor heads with a diameter of 20mm, see Figure 6 left, and another type with small sensor heads with a diameter of 12mm, see Figure 6 right.

Figure 6 Prototype spinner anemometer sonic sensors specifically designed for the spinner anemometer. To the left with classic sensor heads. To the right with small sensor heads.

Each 1D sonic sensor is mounted on the spinner with a fitting that is fixed to the spinner. The sensors are mounted from the inside of the spinner, and the bent tube with the sensor path is lead through the fitting to the outside of the spinner.

In this project the rotor azimuth position was measured with two accelerometers mounted in a plane perpendicular to the shaft and also perpendicular to each other.

3 Concept Tests In Wind Tunnel On a Scaled Spinner Anemometer

3.1 Scaled Spinner Anemometer Set-Up

The spinner anemometer concept was tested in a large 4x4 m^2 wind tunnel. A scaled spinner (for a Bonus 300kW wind turbine) with a spherical nose and a transition to a conical part was mounted horizontally on a shaft on a tripod. The shaft could be rotated up to about 15rpm. The tripod was mounted on a turn-table in the floor which could be yawed to change angle of attach of the wind on the spinner. A cup anemometer was mounted at the lower left corner of the inlet to the test section. The arrangement in the wind tunnel is shown in Figure 7, and a detailed view of the sonic sensors mounted on the spinner is shown in Figure 8. The two different types of 1D sonic sensor shown in Figure 6 were tested.

Figure 7 Arrangement for concept tests in a 4x4 m² wind tunnel. The spinner is seen yawed to -90° and the sonic sensors can be seen on the nose of the spinner. One sensor is horizontal in which position the sensor wind speed was measured with a sweep from -90° to 90° and related to the cup anemometer wind speed measured in the lower left corner of the inlet to the open test section.

Figure 8 1D sonic wind sensors with small sensor heads, mounted from the inside of the spinner through the fittings on the 300kW wind turbine spinner. The sensor paths are tilted backwards in order for the wind to flow undisturbed into the paths. This eliminates flow distortion due to the sensor heads for the most important wind directions when the wind turbine is yawed into the wind.

Unfortunately, the cup anemometer was mounted close to a wedge in the bottom of the outlet, as seen in Figure 7. The wedge introduced a significant speed up in the location of the cup anemometer rotor. This means that all wind speed measurements relating to this cup anemometer had to be corrected. An estimate of the speed up factor was found in the comparison of the theoretical CFD calculations with the wind tunnel measurements. This speed up factor was estimated to a value of 1.35.

3.2 Tests with Non-Rotating Spinner Anemometer

At first, measurements were made without rotation in order to measure the flow characteristics due to flow inclination alone. The spinner was positioned with one sensor horizontal. Figure 9 shows the sensor wind speed relative to the cup wind speed at about 8m/s, measured at varying yaw angles (flow inclination angle), and with a continuous yaw sweep. Figure 10 shows yaw sweeps at three different tunnel wind speeds.
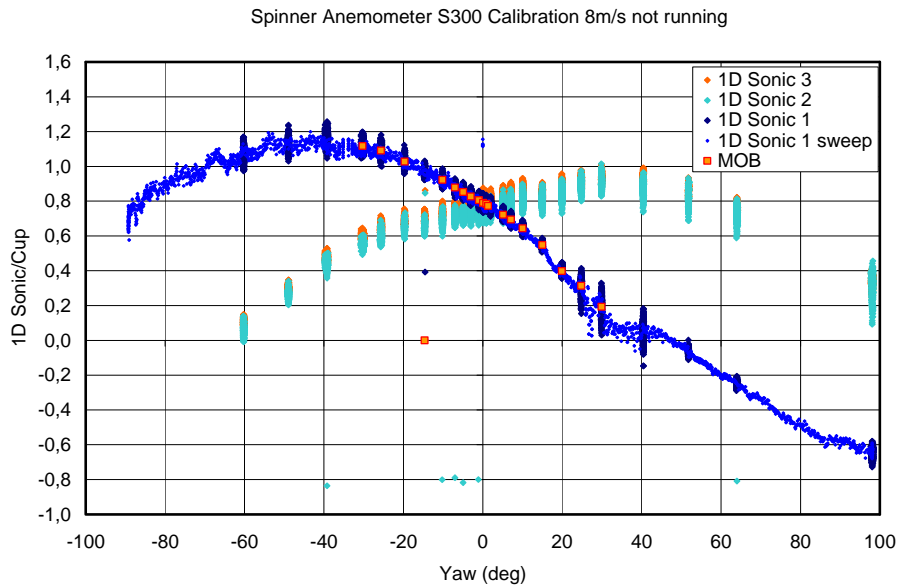
Figure 9 Measurements of 1D wind speeds wit classic sonic sensors relative to corrected cup anemometer wind speed with sensor 1 in horizontal position and with continuous yaw sweep
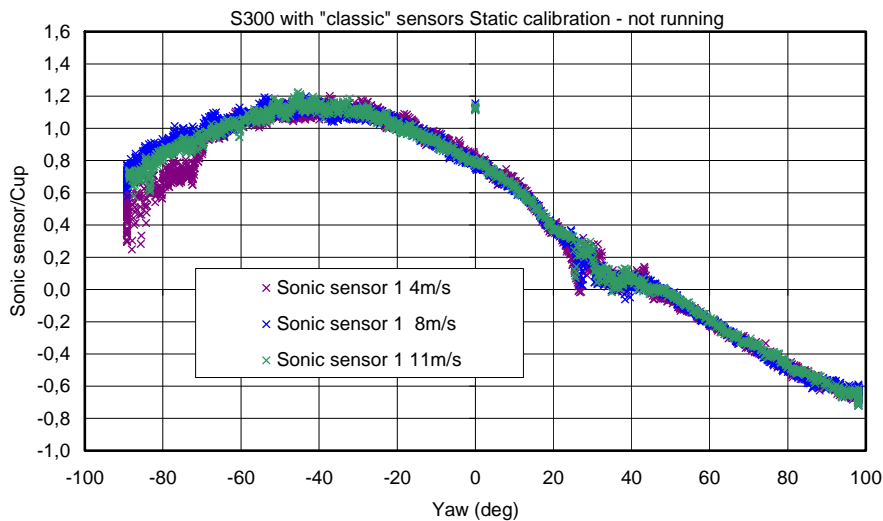

Figure 10 Measurements of 1D wind speed with classic sonic sensor 1 relative to corrected cup anemometer wind speed at three different wind speeds and with continuous yaw sweeps

3.3 Tests While Spinner Rotates

Figure 11 to 18 shows measurements of all three sensors during rotation at 15rpm and a wind speed of 9m/s for yaw angles of 0°, 5°, 10°, 15°, 20°, 28°, 38° and 57°. Figure 13 and 15 at 10º and 20º yaw show additional curves of sensors 2 and 3 where the signals have been applied an internal calibration. This internal calibration was made by collecting a database over 10min. Values of each sonic sensor was bouble-sorted, and linear regression from sensor 2 and 3 to sensor 1 was made. The results are then used as calibration values of sensor 2 and 3.

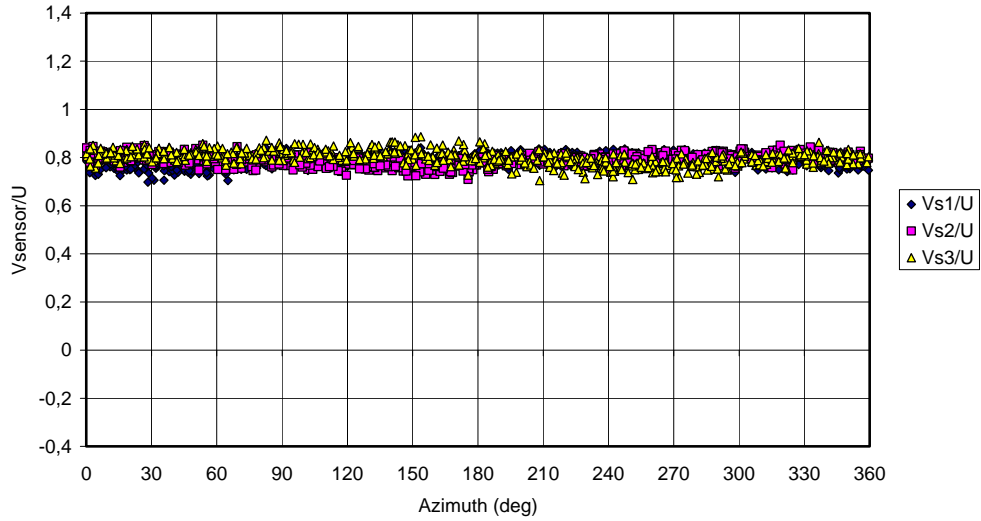Spinner anemometer S300, Classic heads, 0deg yaw, 15rpm

Figure 11 Relation between spinner anemometer sonic sensors (classic) and corrected cup anemometer for a rotational speed of 15rpm and 0° yaw

Spinner anemometer S300, Classic heads, 5deg yaw, 15rpm

Figure 12 Relation between spinner anemometer sonic sensors (classic) and corrected cup anemometer for a rotational speed of 15rpm and 5° yaw

Spinner anemometer S300, Classic heads, 10deg yaw, 15rpm

Figure 13 Relation between spinner anemometer sonic sensors (classic) and corrected cup anemometer for a rotational speed of 15rpm and 10° yaw

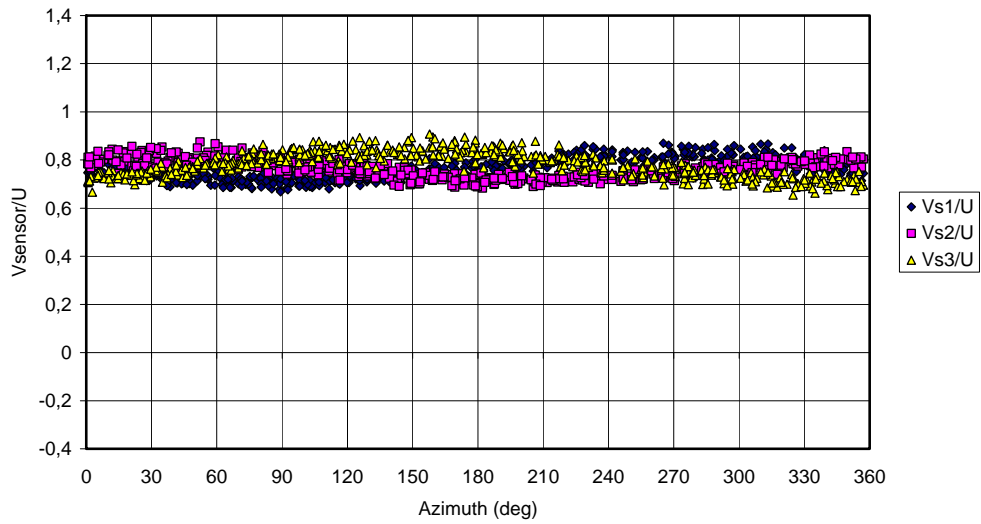Spinner anemometer S300, Classic heads, 15deg yaw, 15rpm

Figure 14 Relation between spinner anemometer sonic sensors (classic) and corrected cup anemometer for a rotational speed of 15rpm and 15° yaw

Spinner anemometer S300, Classic heads, 20deg yaw, 15rpm
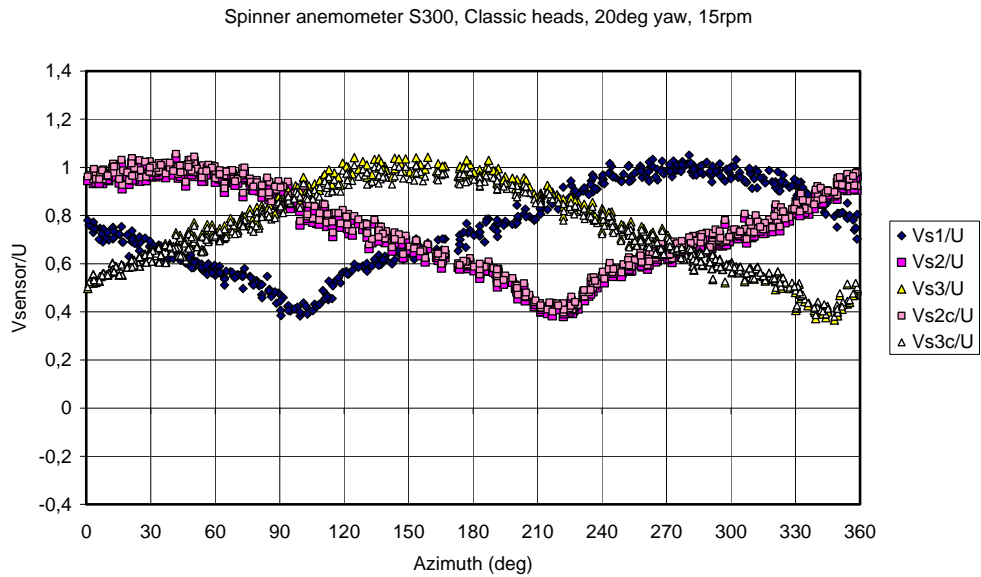
Figure 15 Relation between spinner anemometer sonic sensors (classic) and corrected cup anemometer for a rotational speed of 15rpm and 20° yaw

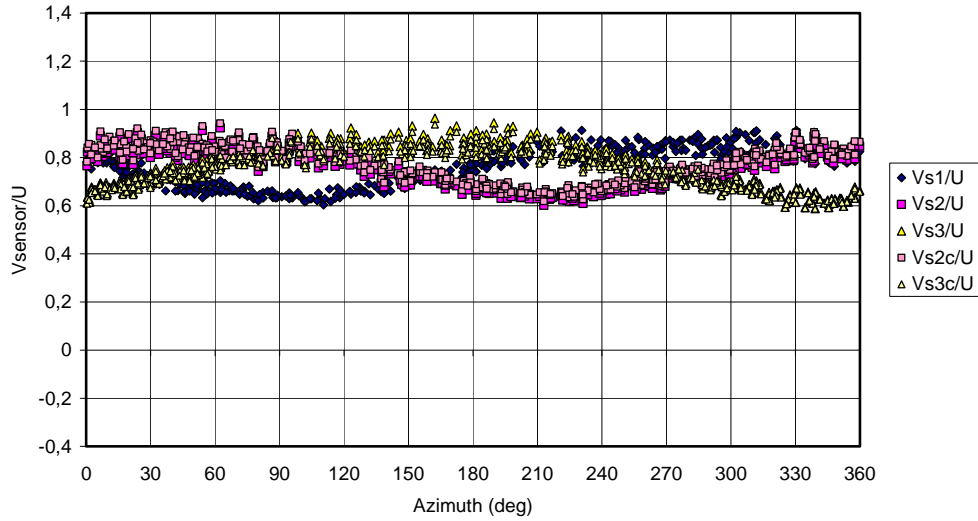Spinner anemometer S300, Classic heads, 28deg yaw, 15rpm

Figure 16 Relation between spinner anemometer sonic sensors (classic) and corrected cup anemometer for a rotational speed of 15rpm and 28° yaw

Spinner anemometer S300, Classic heads, 38deg yaw, 15rpm
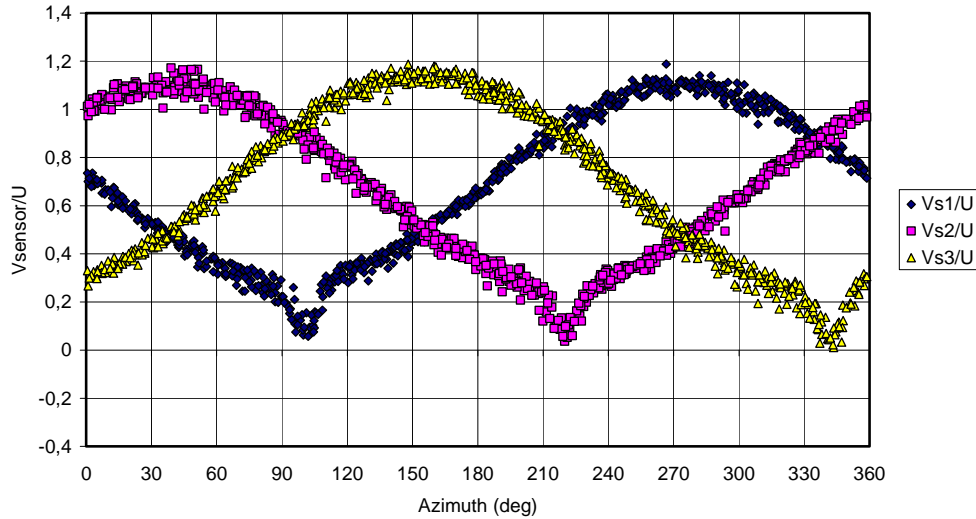
Figure 17 Relation between spinner anemometer sonic sensors (classic) and corrected cup anemometer for a rotational speed of 15rpm and 38° yaw

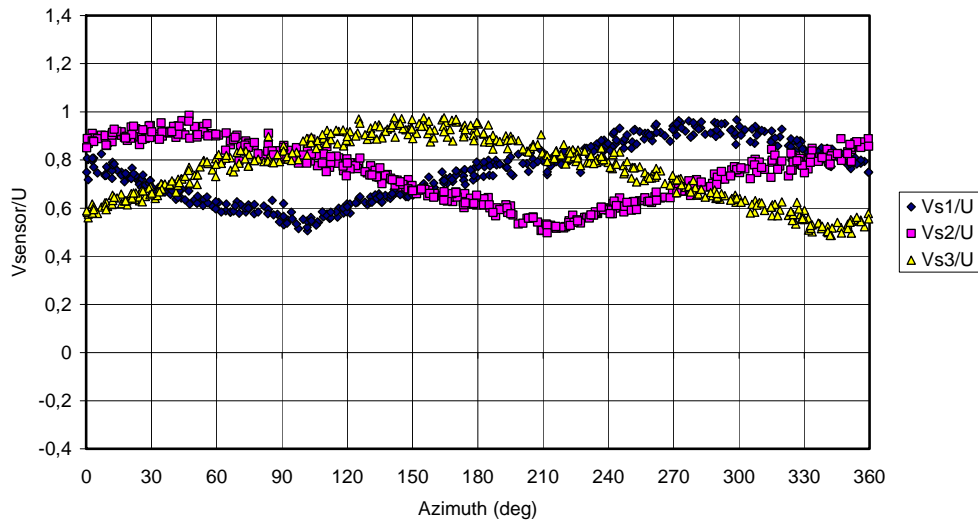Spinner anemometer S300, Classic heads, 57deg yaw, 15rmp
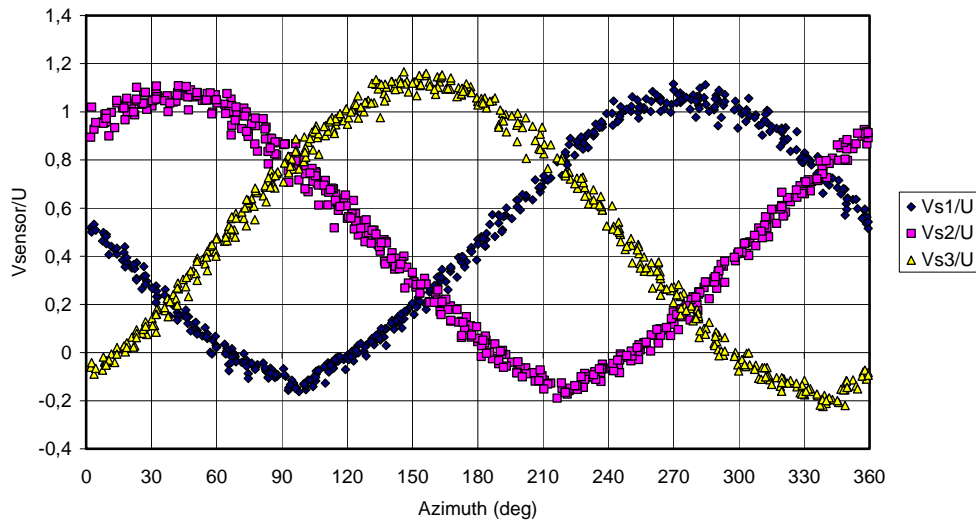
Figure 18 Relation between spinner anemometer sonic sensors (classic) and corrected cup anemometer for a rotational speed of 15rpm and 57° yaw
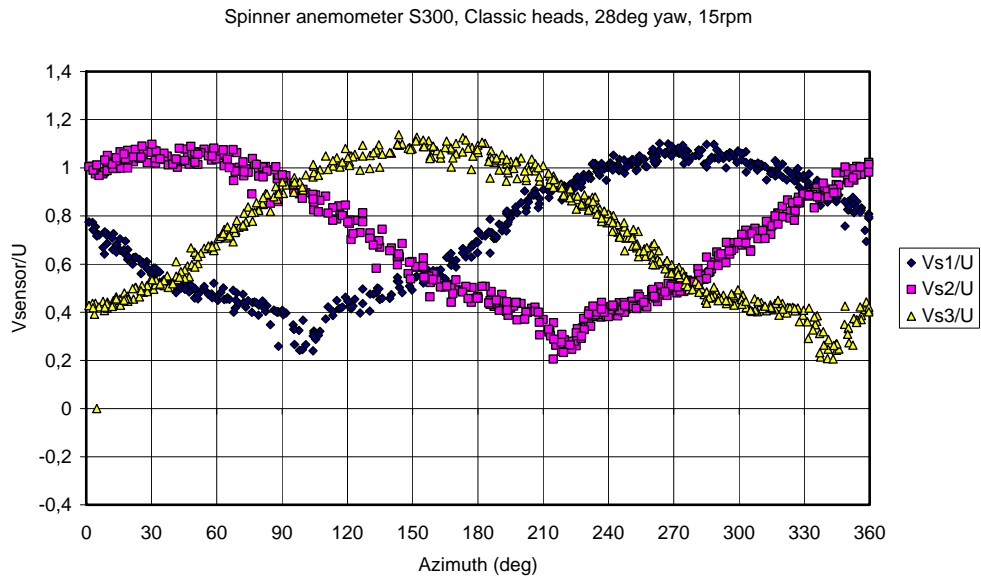
4 Investigation of Flow over a Wind Turbine Spinner by the Use of CFD

The flow over the spinner of a wind turbine was investigated by CFD analysis. Detailed description of setup of the flow solver and the results are reported in [5]. Here, the main results are described.

4.1 Computational considerations

The flow solver EllipSys3D was used in all computations. The turbulence in the boundary layer was modelled by the k-ω SST eddy viscosity model. In order to simulate

the rotation of the spinner, a non-zero velocity was specified at the wall of the spinner. Figure 19 shows a 3D drawing of the scaled 300kW spinner with the sonic sensors with classic sensor heads mounted.

*Figure 1*9 *The sonic sensors with classic sensor heads mounted on the S300 spinner.*

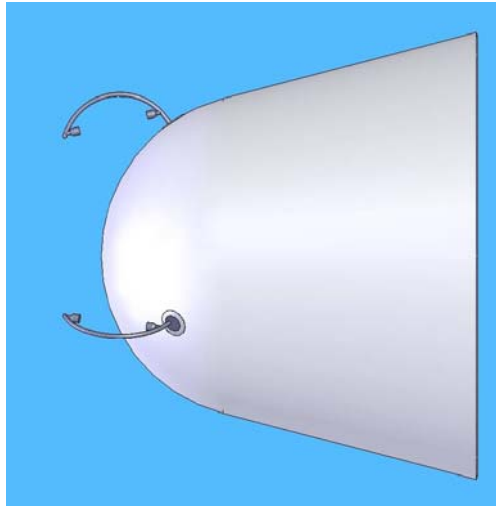The flow calculations were not compared directly with the wind tunnel measurements. The sonic sensors measure the average wind speed over the sensor path from one sensor head to the other. The calculations were not averaged over the same path. Instead, the wind speed was averaged over a cylinder as shown in figure 20 and 21. Figure 20 shows the sensor path projected into a cylindrical wind speed volume, and Figure 21 shows the volume in front of the spinner. The volume of the circular cylinder has a radius of 312 mm from the axis of the spinner, extending from 70 mm upstream of the nose of the spinner, to 95 mm downstream of the nose, see Figure 21.
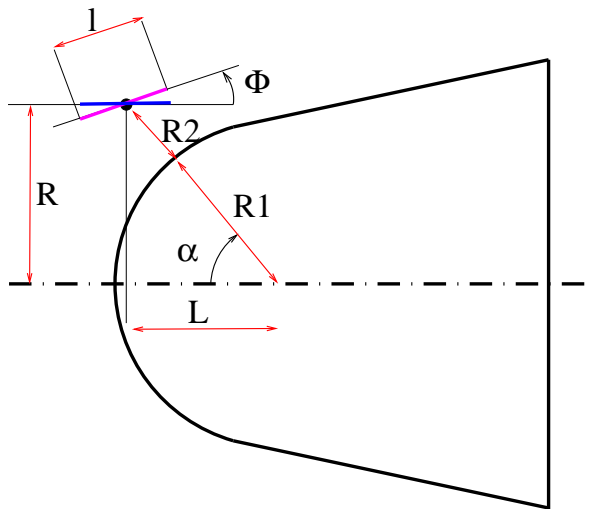

Figure 20 The geometrical quantities used to compute the sensor position. In the measurements, the sonic sensor path is the magenta curve with length l, while in the computations the path is the blue line with length l*cos(Φ) is used instead.
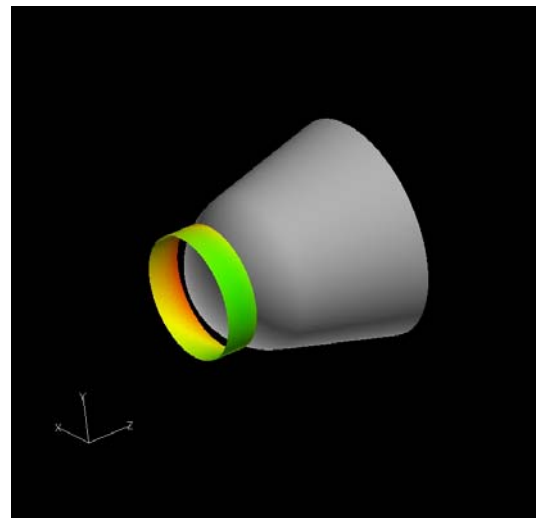
Figure 21 To emulate the measuring volume of the sonic sensors in the experiment, the circular area shown was used in the computations.

The computational mesh was made with the GridGen mesh generation code. The surface mesh on the spinner is show in Figure 22, right. The 3D volume mesh was generated using the Risø enhanced hyperbolic mesh generator HypGrid3D. For the S300 spinner, 256 cells are used around the spinner in the cross stream direction, and 64 cells in the flow direction, and two additional square blocks of 64x64 cells are placed at the nose and rear of the spinner, respectively. The number of cells in the normal direction is 64, giving a total cell count of approximately 1.6 million cells.

When modelling the scaled S300 spinner in the computations, the geometry was as shown in Figure 22. But in contrast to the measurements that were performed in the tunnel, the support structure was not included in the computations, and the base of the spinner was modelled as a closed surface.
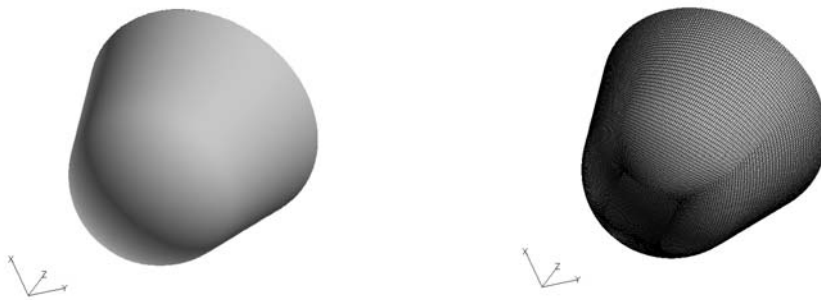
Figure 22 Perspective view ofS300 spinner. To the right the surface mesh have been applied.

An identical topology is used for the S3600 spinner of a 3,6MW wind turbine. In this case the nacelle is included in the calculations, and 128 cells are used in the flow direction, and 128 cells are used in the normal direction, see Figure 23. The total number of cells for the S3600 mesh is approximately 5.2 million cells, see Figure 24. An example of calculated flow lines for a 45° skew airflow is shown in Figure 25.
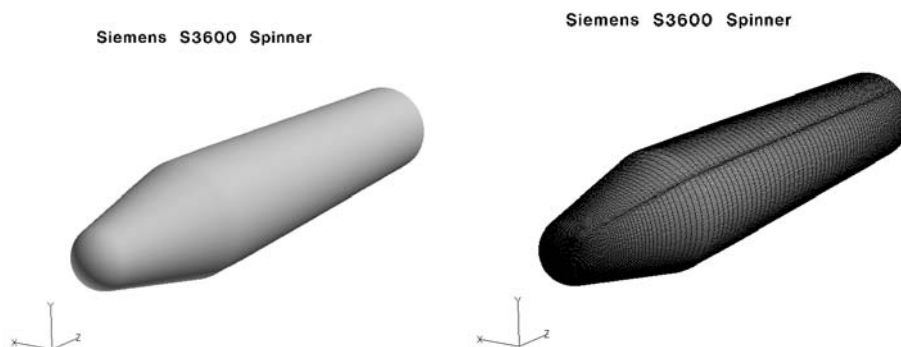
Figure 23. Surface mesh for the S3600 spinner and nacelle.

Figure 24 Cross sectional cut in the mesh grid around the S3600 3.6MW wind turbine spinner and nacelle
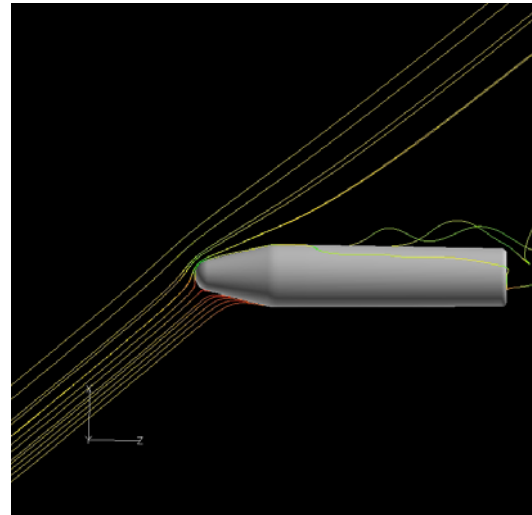
Figure 25 The flow around the 3.6MW wind turbine spinner for a yaw error of 45 degrees, the highly separated flow on the lee side of the nacelle is clearly visible.

Boundary Conditions

To avoid influence of location of the outer boundary, the boundary is located more than 10 diameters away from the spinner. Most of the outer boundary is specified as inlet, where the velocity and turbulent quantities are specified. The part of the outer 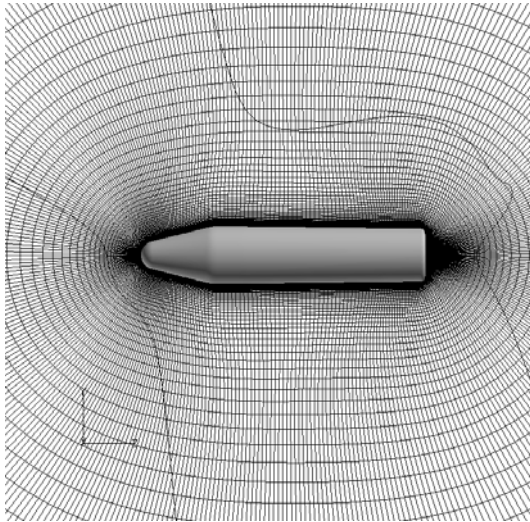spherical domain located directly downstream of the nacelle was specified as outlet, assuming a fully developed flow. Finally, no slip conditions are given at the surface of the spinner. For the rotating cases, a boundary velocity according to the rotation of the spinner is used, for the non-rotating cases a zero velocity at the surface is prescribed. In the case of yaw angles above 60 degrees, the outlet part of the boundary is moved to accommodate the outflow.

Definitions of coordinate systems

In the CFD computations on the spinners the spinner rotation is in counter clockwise direction when seen along the flow direction. The azimuth angle is measured from the x-axis with positive direction in the clockwise direction. Zero yaw corresponds to flow along the z-axis, and positive yaw corresponds to adding a positive x-component to the flow, see Figure 26. Note that these definitions are specific to the CFD calculations alone.

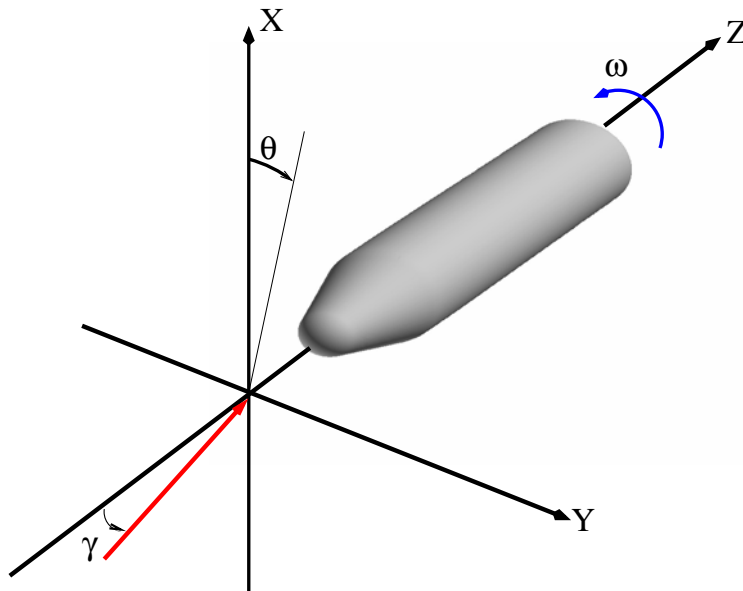*Figure 26. Definitions in the CFD calculations of the yaw angle (γ in the vertical xz-plane), the azimuth angle (θ in the xy-plane) and the positive rotational direction around the z-axis (ω) for the spinner computations. The figure shows the modelled S3600 spinner.*

4.2 Computations on S300 Spinner

Computations on the S300 spinner was made for yaw angles 0°, 10° and 20°. Both for the 10° and 20° yaw cases, a series of computations were performed to obtain good overall agreement of the velocity, see table 1

Table 1 The operational conditions for the S300 spinner used in the computations

Velocity [m /s]	RPM	Yaw angle [deg]
6.5	0	20
7.5	0	10
8	0	10
10	0	0
10	0	10
10	0	20
7.5	15	10
10	15	0
10	15	10
10	15	20

The outcome of the investigation was twofold. Firstly, a free stream velocity was determined that makes the computations agree with the measured values, which had an error due to speed up at the position of the cup anemometer. Secondly, it was seen that the same results could be obtained by a simple scaling of the velocities with a factor. Additionally, it was seen that the rotation of the spinner has a very weak influence on the measured velocity profiles, and can easily be ignored for practical purpose. This conclusion is valid for an axis symmetric configuration, but may very well not be valid for an eccentric setup of the spinner.

Due to the physical design of the sonic sensors flow from some directions will be distorted by the sensor itself. When the flow is hitting the supporting bent tube before it reaches the sensor path, the wake from the tube will disturb the measurement. This influence is not very evident in the wind tunnel measurements, but it must be part of the distortion of the curves between yaw angle from 20° and 40° and onwards to 100°.

When the flow is along the sonic sensor paths one sensor head will distort the flow in the path. This well-known effect, "sensor head flow distortion" [9], influences on the wind speed measurement at flow angles relative to the sensor path up to about 20°. Looking at the measured sensor wind speeds in Figure 15, 16 and 17for yaw angles of 20°, 28° and 38°, respectively, this sensor head flow distortion effect is quite evident in the wind tunnel measurements. The dips in the curves due to the flow distortion effect are expected at azimuth angles of about 90°, 210° and 330°, but they occur at about 100°, 220° and 340°. This is caused by a 40° offset difference in the azimuth definition.

In the CFD computations, the sensor heads are not modelled, and the computations thus say nothing about the flow distortion by the sensor itself.

Figure 27 shows the results of CFD calculations on the S300 spinner for two different wind speeds, and for rotation and stand still.

Figure 27 Comparison of computed and measured sensor path wind speeds on the S300 spinner for 10° yaw angle. The calculated curve (W=10 [m/s]) is scaled with a factor 0.75 to compare with the other two calculated curves at 7.5m/s. The measurements were made with a free wind speed of about 6.5m/s.

Figure 27 for a yaw error of 10° shows that the differences between the calculated curves are very small. This indicates that the influence of rotation versus non-rotation is very little. It also indicates that the difference between 7.5m/s and the scaled 10m/s is very little, and thus shows that the wind speeds are scalable. The measured curve is not directly comparable because it is measured at a lower wind speed. At 20° yaw error, see Figure 28, the curves are more comparable because they compare at the same wind speed about 6.5m/s. Here, the calculated curves almost collapse into the same curve, and

confirm what was concluded from the 10° yaw error case, that the differences between rotation and non-rotation and is very little, and that the wind speeds are scalable.

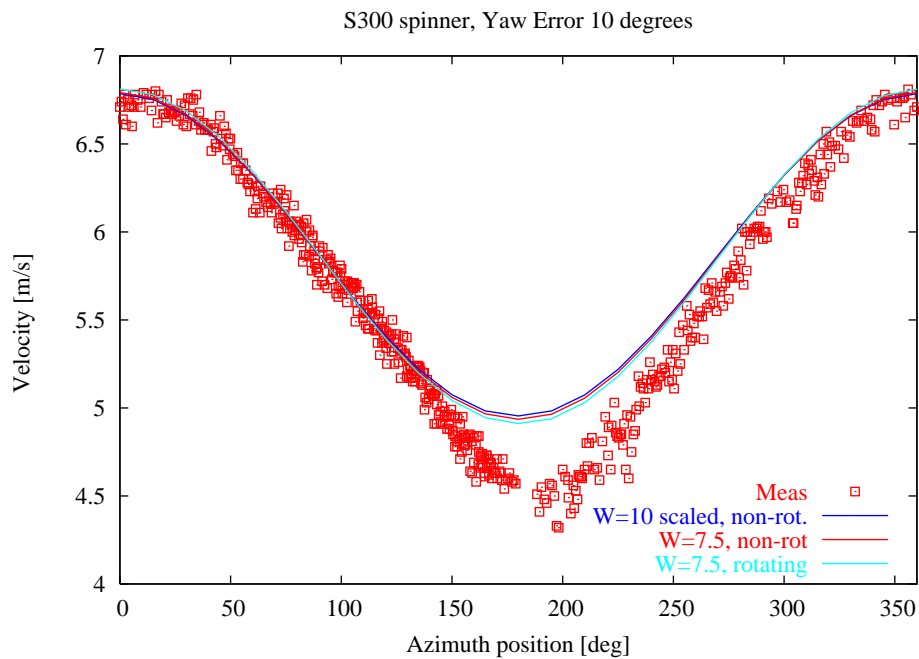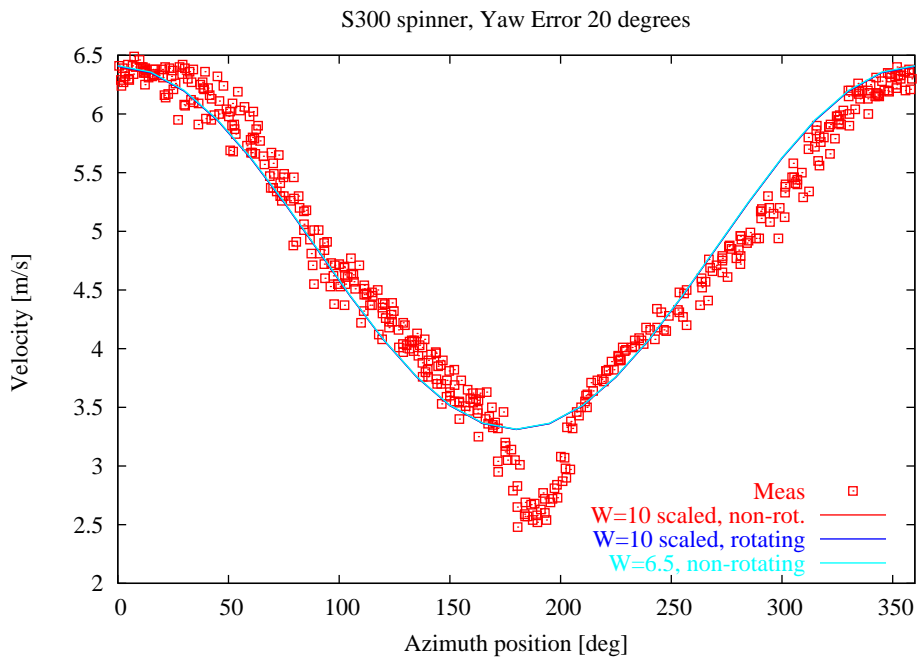*Figure 28 Comparison of the computed and measured sensor path wind speeds on the S300 spinner for 20° yaw angle. The calculated curves (W=10 [m/s]) are scaled with a factor 0.65 for comparison with the calculated curve and at 6.5m/s and the measured curve at about 6.5m/s.*

Figure 29 shows calculated sensor path wind speeds for yaw angles from 0° to 80° at 8m/s. The curves are seen to go from a straight line at 8m/s to a cosine with decreasing average value over one rotation.
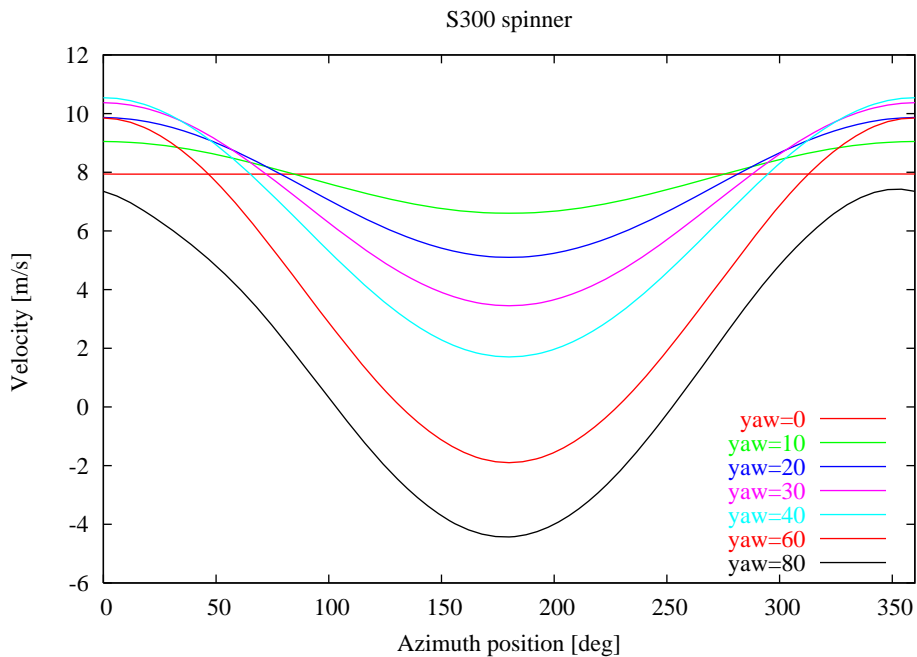
Figure 29 The computed sensor path wind speeds on the S300 spinner for 0°, 10°, 20°, 30°, 40°, 60°, 80° yaw cases at 8m/s free wind speed.

4.3 Computations on S3600 spinner

The computations on the S3600 spinner and nacelle were performed for 10m/s and for yaw angle between 0° and 180°. Two different positions of the sonic sensors on the spinner were investigated, at 45° and 55°. The sensor path wind speeds for varying azimuth positions are shown in figure 30 and 31.
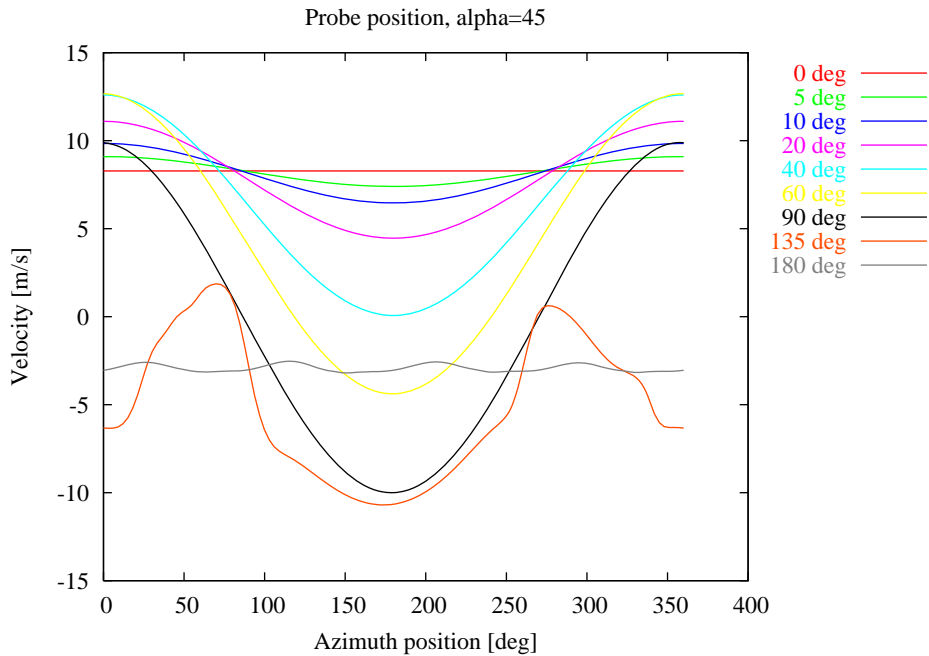
Figure 30 The sensor path wind speed with azimuth variation for a sensor position angle of 45°.
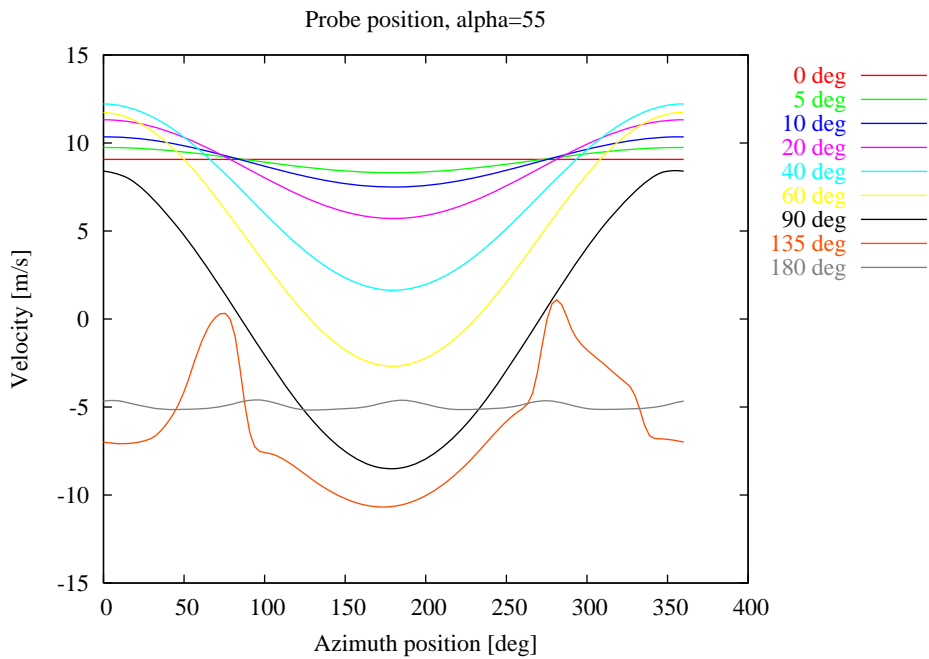
Figure 31 The sensor path wind speed with azimuth variation for a sensor position angle of 55°.

Figure 30 and 31 show the same kind of patterns for the sensor path wind speeds. At 55° the wind speeds are a little higher because the sensor positions are further back on the spinner where the air speed has increased.

5 Spinner Anemometer Conversion Algorithm

5.1 Conversion Algorithm for 3D Measurements

Having verified that the CFD method is capable of reasonably predicting the behaviour of the flow around the spinner, except for the sensor head shadow effect, the series of computations for different yaw settings was used for development of an algorithm that was able to convert the sensor path wind speed measurements back to the original parameters: free wind speed, angle of attack relative to the rotor axis and azimuth angle on the spinner.

The calculated responses in Figure 29, 30 and 31 indicate that the responses are cosine shaped at least for yaw angles below 90°. The curves appear to be of a family of curves that reduce the average sensor wind speed over one revolution with increasing yaw angle while the amplitude increases. The average wind speeds over one revolution are seen to decrease very little at small yaw angles but the decrease is rapid closer to 90°, where it actually is zero. This indicates a cosine relation of the average value. The opposite is the case for the amplitude, which seem to increase with a sinus. The path wind speed of one sonic sensor can indeed be expressed as a simple function of the flow angle to the rotor axis α, the azimuth position φ, the free wind speed U, and two constants K_1 and K_2:

$$V_S = U(K_1 \cos \alpha + K_2 \sin \alpha \cos \varphi) \qquad (1)$$

With this expression for one sensor we can express the path wind speed for the three sensors positioned axially symmetric on the spherical nose:

$$V_{S1} = U(K_1 \cos \alpha + K_2 \sin \alpha \cos \varphi) \qquad (2)$$

$$V_{S2} = U(K_1 \cos \alpha + K_2 \sin \alpha \cos(\varphi + 2\pi/3)) \qquad (3)$$

$$V_{S3} = U(K_1 \cos \alpha + K_2 \sin \alpha \cos(\varphi + 4\pi/3)) \qquad (4)$$

With the assumption of these expression of the sensor path wind speeds the inverse problem, where the sensor path air speeds are known and the wind conditions are to be determined, has a simple solution. The three expressions of sensor path wind speeds have three unknowns, the azimuth angle of the stagnation point on the spinner φ, the flow angle of the stagnation point to the rotor axis α, and the free wind speed U.

The azimuth angle is expressed by:

$$\varphi = Ar\tan \frac{\sqrt{3}(V_{S2} - V_{S3})}{V_{S2} + V_{S3} - 2V_{S1}} \qquad (5)$$

The flow angle to the rotor axis is expressed by:

$$\alpha = Ar\tan \frac{K_1(V_{S2} - V_{S1})}{K_2(V_{S1} \cos(\varphi + 2\pi/3) - V_{S2} \cos \varphi)} \qquad (6)$$

And the wind speed by:

$$U = (V_{S1} + V_{S2} + V_{S3})/(3K_1 \cos \alpha) = U_{ave}/(K_1 \cos \alpha) \qquad (7)$$

The azimuth angle φ depend on the three airspeeds alone, and is independent of the constants K_1 and K_2. The wind speed is proportional to the average of the three sensor wind speeds, and is dependent on the flow angle to the rotor axis α. These

equations are reasonably simple to apply for an algorithm of the spinner anemometer. The CFD calculated sensor wind speeds for appropriate values of K_1 and K_2. of the spinner anemometer S300 are compared to the sonic sensor expression (2) in figure 32. They compare extremely well up to 60º. Only at 80º the function values deviate from the CFD calculations.
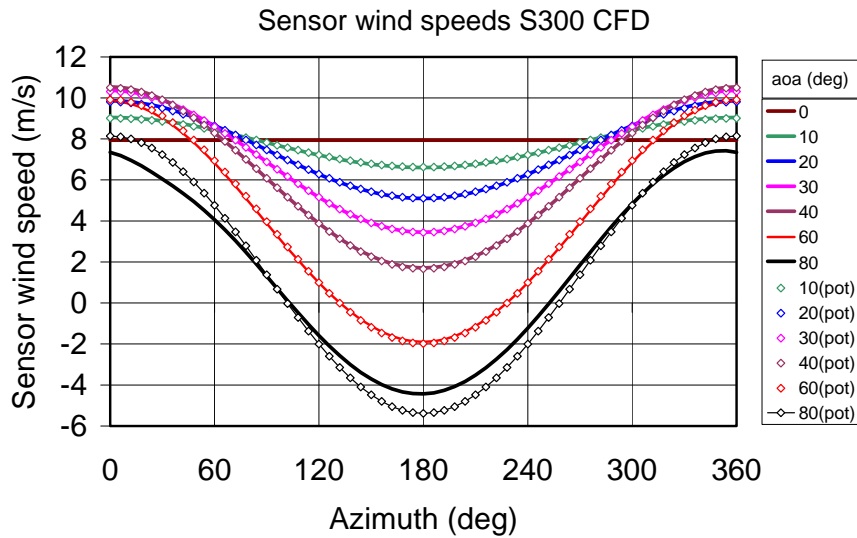

Figure 32 The computed sensor path wind speeds on the S300 spinner for the 0º, 10º, 20º, 30º, 40º, 60º, 80º yaw angles and 10m/s free wind speed, and the values from formula (2).

With the same K_1 and K_2. values the CFD calculations are compared to the wind tunnel measurements in Figure 33 for 10° yaw and in Figure 34 for 20° yaw. The cup anemometer measurements have in this case been applied a correction factor of 0.74. With this correction the calculated values compare quite satisfactorily to the measured values.

Figure 33 Measured sensor wind speed (classic sensor heads) versus free wind speed for the S300 spinner for 10° yaw angle compared to formula (2) derived from CFD calculations.

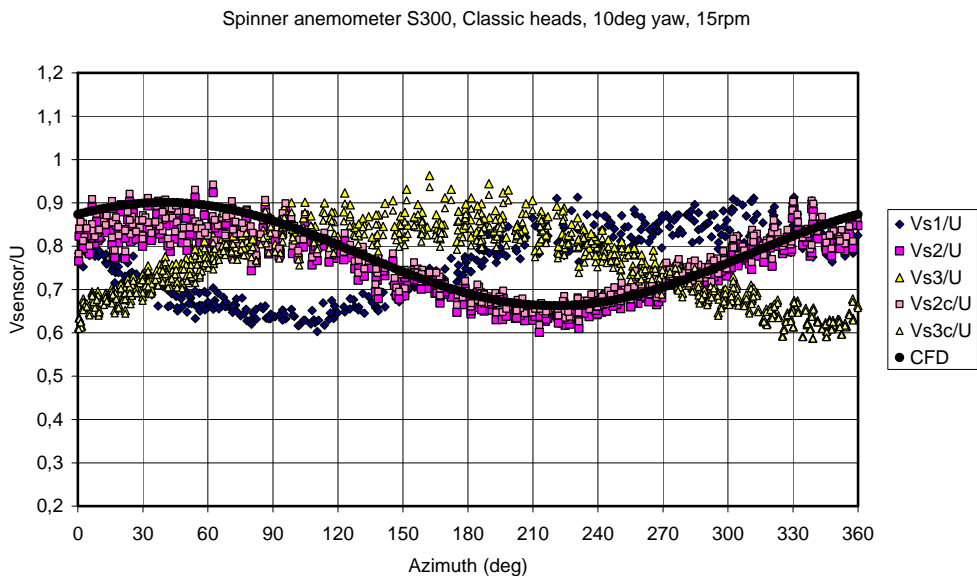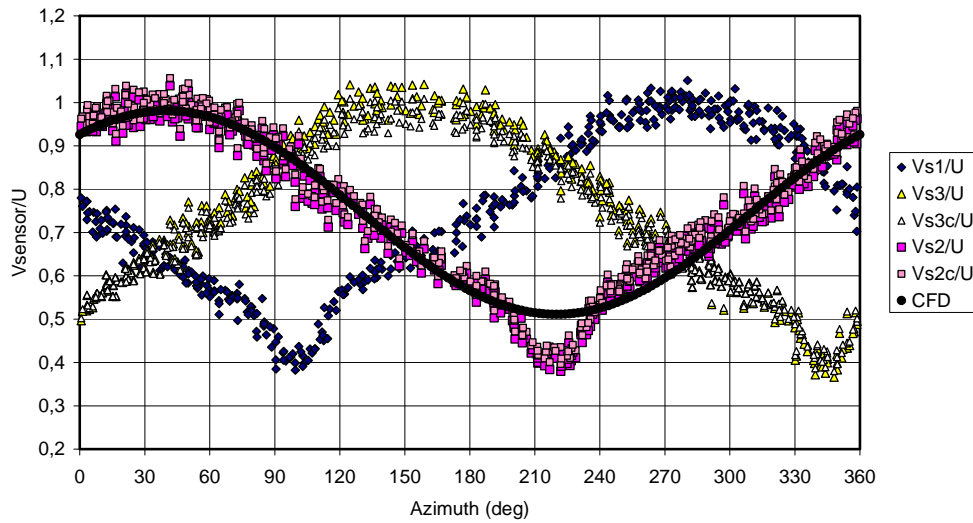*Figure 34 Measured sensor wind speed (classic sensor heads) versus free wind speed for the S300 spinner for 20° yaw angle compared to formula (2) derived from CFD calculations.*

6 Field Tests on Scaled Spinner Anemometer

The S300 spinner anemometer was tested under field conditions at the Risø test site. In this case only the "new" sensors were used in order to reduce the sensor head shadow effect.

6.1 Free field experimental setup

A 3D Gill Windmaster sonic anemometer was mounted with the sensor heads at same height and about three meters to the side and a little in front of the spinner anemometer for comparison tests. Measurements were made while rotating at 15rpm. The whole arrangement of the spinner and sonic sensors are shown in figure 35 and the two sensors are shown in figure 36.

Figure 35 Arrangement of the S300 spinner anemometer with "new" sensors in comparison with the sonic anemometer at Risø test site

Figure 36 The S300 spinner anemometer and the Gill Windmaster in comparison

6.2 Comparison of spinner anemometer with 3D sonic anemometer

Time traces lasting 100 seconds of the two wind sensors are shown in figure 37, 38 and 39. Figure 37 shows comparison of scalar winds, while figure 38 shows comparison of yaw angles, and figure 39 comparison of flow inclination angles. The measured wind speeds and wind directions by the two anemometers seem to follow each other quite well. The most significant variations are the same for the two sensors. The 10min average absolute wind speed of the 3D sonic is only 2% lower than the spinner anemometer wind speed for the time trace, of which is shown only 100secs in figure 36. Figure 40 and 41 show compared average wind speeds and standard deviations over a 3 hour measurement period. Average values have a slope of 0.975, and the standard deviations 1.045.
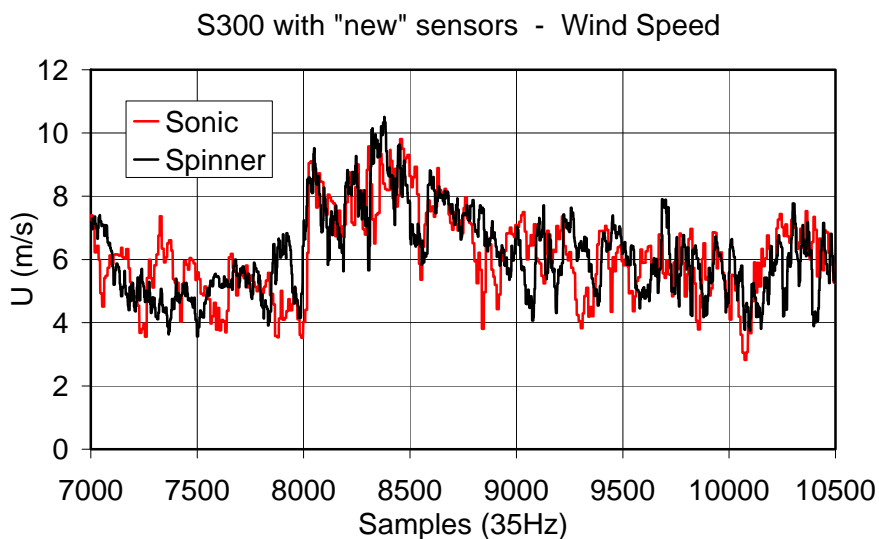

Figure 37 Comparison of measured wind speeds at 35Hz sampling rate (100sec of data) of S300 spinner anemometer and 3D sonic anemometer
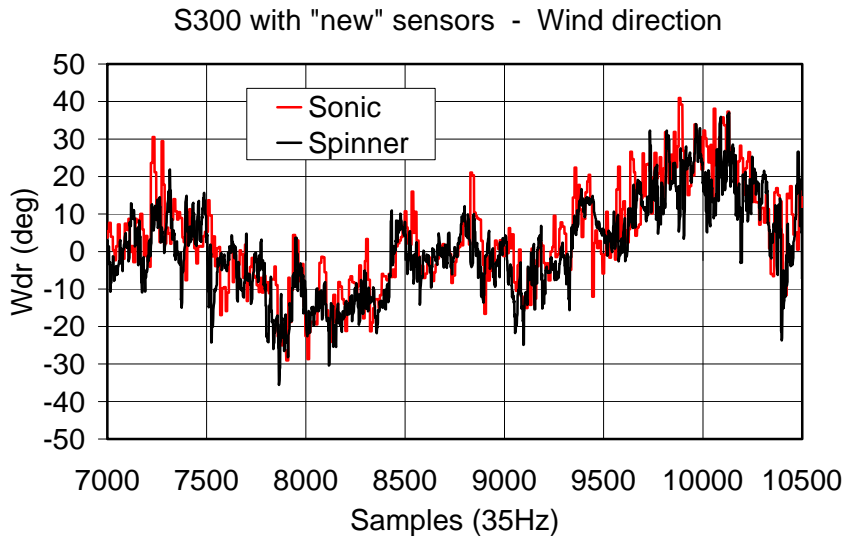
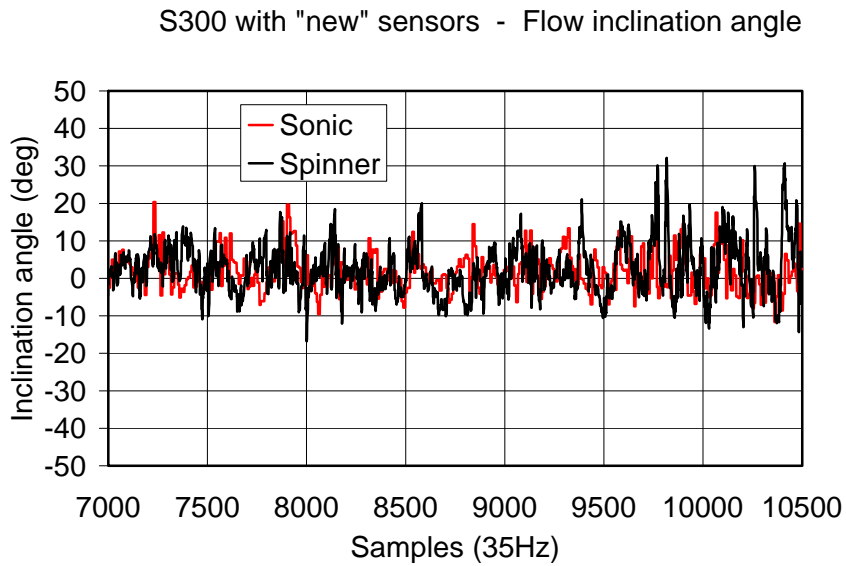*Figure 38 Comparison of measured wind direction at 35Hz sampling rate*

Figure 39 Comparison of measured flow inclination angle at 35Hz sampling rate

3D sonic versus S300 with "new" sensors
- 10min average values

y = 0,9749x
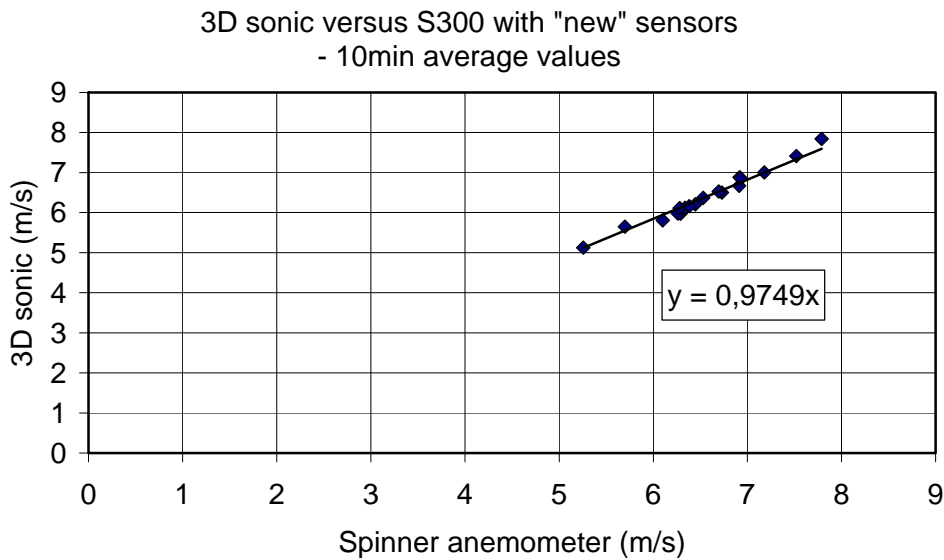
Figure 40 10min average wind speed values of S300 spinner anemometer versus Gill Windmaster 3D sonic

3D sonic versus S300 with "new" sensors
- 10min standard deviation values

y = 1,0454x
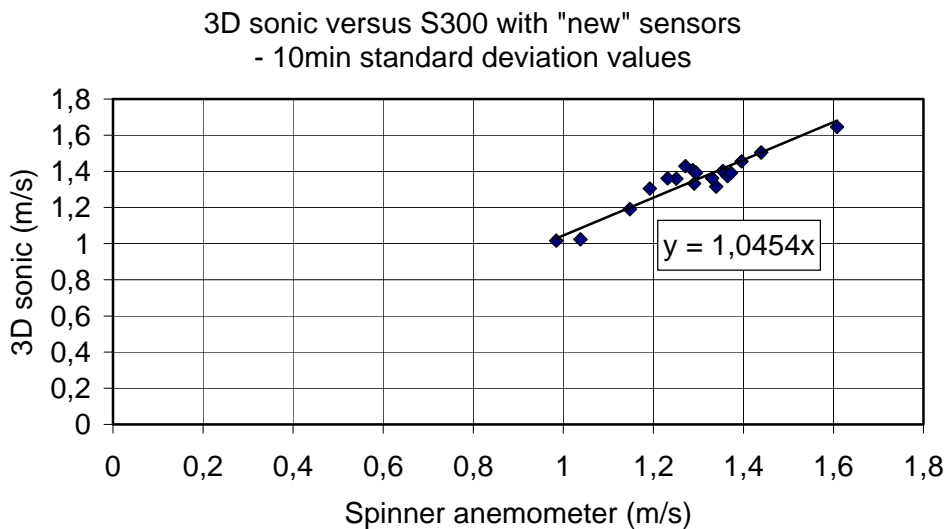
Figure 41 10min stddev wind speed data of S300 spinner anemometer versus Gill Windmaster 3D sonic

6.3 Comparison of Measurements Based on 1D Conversion Algorithm

The spinner anemometer is normally operated with three 1D sonic sensors. This ensures that instantaneous wind speed, yaw error and flow angle are measured. But the spinner anemometer can in principle be operated with only one 1D sonic sensor. Each sonic sensor rotates and delivers measured wind speeds from all azimuth positions. Over time these wind speeds can give comparable values to the average values from the 3D wind measurement. Figure 42, 43 and 44 shows how measurements performed with only on 1D sonic sensor compares to measurements with all three sensors using the conversion algorithm from chapter 5. The averaging time for the moving average signal is about 30sec.

Spinner anemometer S300 Wind Speed
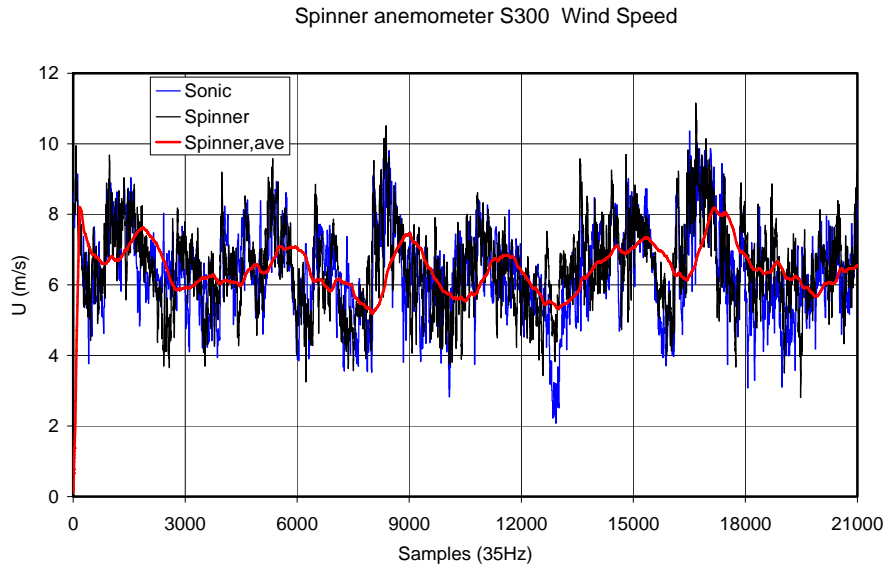
Figure 42 Comparison of measured wind speed at 35Hz sampling rate (10min of data) of spinner anemometer and 3D sonic anemometer

Spinner anemometer S300 Wind direction
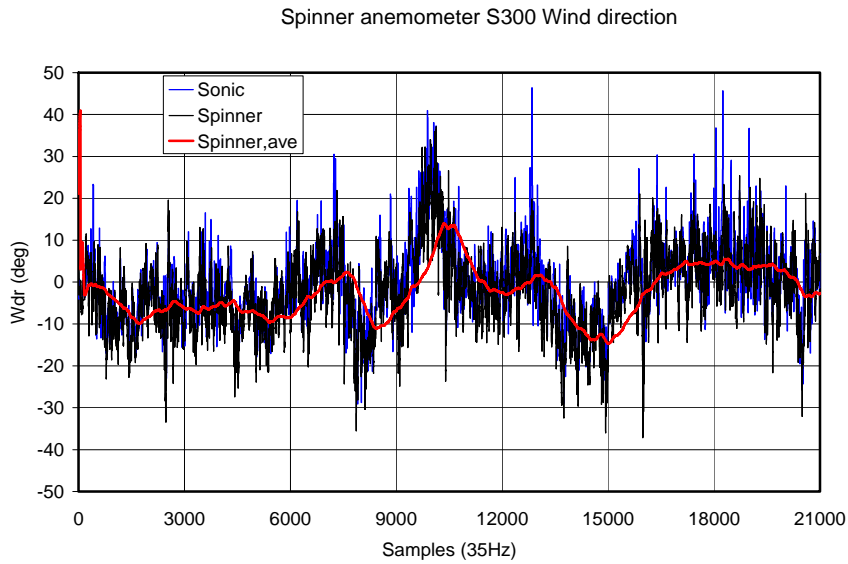
Figure 43 Comparison of measured horizontal inflow angle at 35Hz sampling rate (10min of data) of spinner anemometer and 3D sonic anemometer

Flow inclination angle
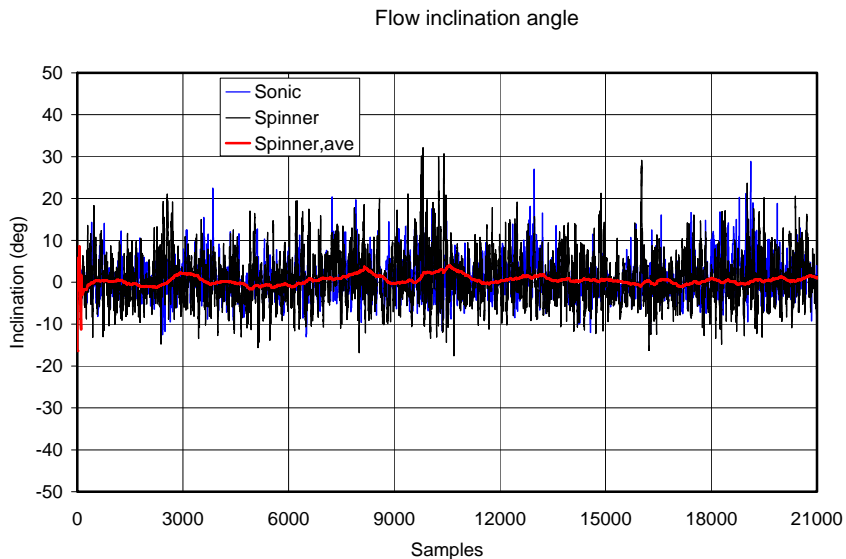
Figure 44 Comparison of measured vertical inflow angle at 35Hz sampling rate (10min of data) of spinner anemometer and 3D sonic anemometer

7 Field Tests on Full Scale Spinner Anemometer

The prototype spinner anemometer with small sensor heads was put onto a 3.6MW wind turbine spinner S2300, see figure 45 and 46. The spinner anemometer was connected to a separate data acquisition system, and measurements were started in March 2007. The spinner anemometer has been operated on the wind turbine for more than one year, and significant experience from this year of operation has been gained.

Figure 45 The three 1D sonic sensors mounted on the nose of the 3,6MW wind turbine spinner at the Risø DTU Høvsøre test site.
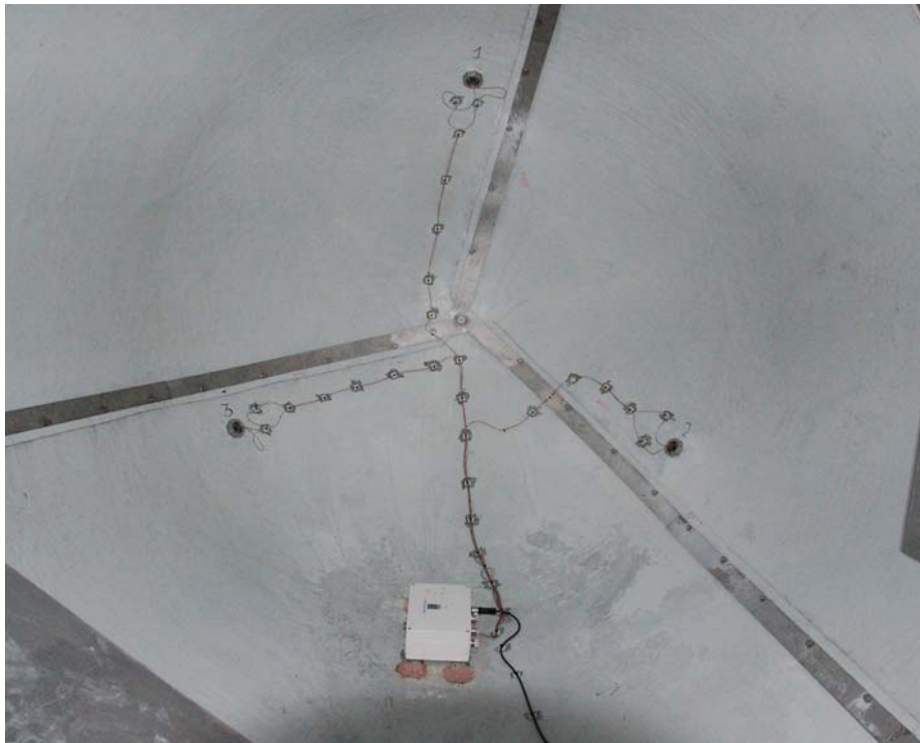
Figure 46 The spinner anemometer as seen from the inside of the spinner. The three 1D sonic sensors are mounted rotationally symmetric on the spinner and are connected to the electronic conversion box, seen in the bottom.

7.1 Internal Calibration of Spinner Anemometer Sensors

In practice, the sonic sensors do not give fully comparable values regarding average and amplitude of the signals due to imperfections. There are a range of geometric variations that influence on each sensor output: inaccuracies of spinner geometry, off-axis mounting of the spinner, and mounting inaccuracies of each sonic sensor. This includes in-accurate position on the spinner surface and tilting and orientation angle of the sensor, which may be due to local surface irregularities on the spinner or mounting irregularities. At least one such irregularity is known, because at least one sensor was offset 2° in forward direction due to a mounting error. All inaccuracies and irregularities may be calibrated and corrected for after installation of the spinner anemometer. This internal calibration is performed by rotating the spinner at a certain inflow angle so that each sonic sensor is exposed to a range of wind speeds within a short time interval, and in principle they will statistically share the same wind variations. Data of each sonic sensor are filtered according to their wind speed value, "Bubble-sorting", and data of sensor 2 and 3 are linear regressed on data of sensor 1. The linear calibration values, gain and offset, are then used to correct sensor 2 and 3 so that their values correspond to the value of sensor 1.

For the spinner anemometer on the 3.6MW wind turbine, the internal calibration was performed on two 30min sets of values, and the average for one hour was determined, see table 2. The measured sonic sensor wind speeds during normal operation at about 6m/s are shown in figure 47. The corrected wind speeds using the internal 60min calibration values from table 2 are also shown in figure 47.

Table 2 Internal calibration of sonic sensors accounting for spinner and mounting inaccuracies

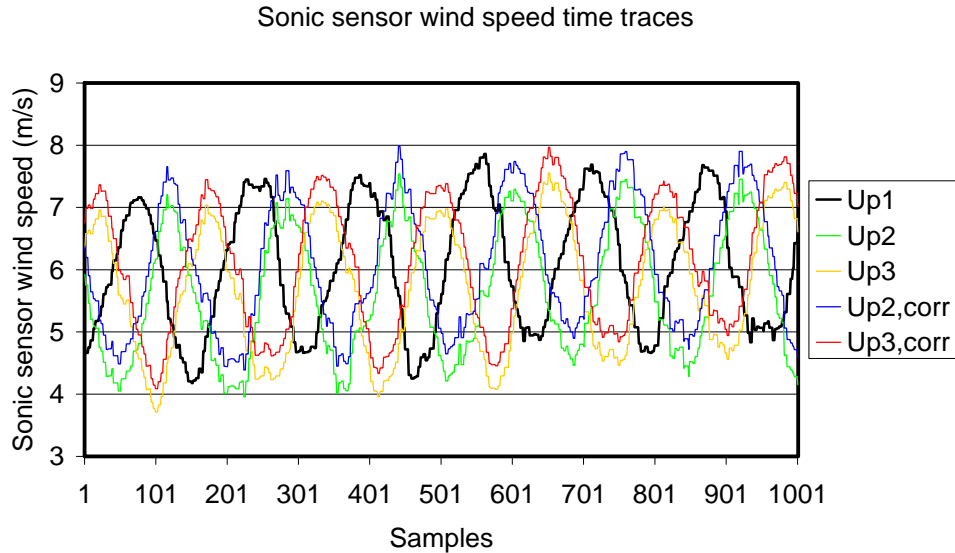|	Sensor 2 versus 1		Sensor 3 versus 1	
	slope	offset	slope	offset
30min (record 1)	1.00586	0.40224	1.00775	0.34641
30min (record 2)	1.00237	0.43466	1.01217	0.32966
60min (average of 1 and 2)	1.00412	0.41845	1.00996	0.33804

Sonic sensor wind speed time traces

Figure 47 Measured path wind speeds of sonic sensors during normal operation. Sensor 1 (black) is not corrected, while sensor 2 (blue) and sensor 3 (read) are corrected with internal calibration values

7.2 CFD calibration of Spinner Anemometer Constants

The aerodynamics of the flow over a spinner and the characteristics of the spinner anemometer were found to have a general and simple expression which could be reversed for a conversion algorithm that converts the three sonic sensor wind speeds to a free wind speed, a yaw error and a flow inclination angle.

The relation between the flow wind speed in the path of one sonic sensor V_S and the free wind speed U, the azimuth angle of the stagnation point of the flow on the spinner φ, and the flow angle to the shaft axis α is expressed as:

$$V_S = U(K_1 \cos\alpha + K_2 \sin\alpha \cos\varphi) \qquad (8)$$

The relation is based on the two constants, K_1, the average factor, which essentially expresses sensitivity to the average value of the wind speed and K_2, the amplitude factor, which is essentially sensitive to the wind transversal to the shaft axis.

The two constants were determined by the CFD calibration approach. In this case, the calculations included the influence from the nacelle, but excluded the influence from the blade roots, profiled blades and the tower. The CFD calculations were made for positions of the sonic sensors on the spinner surface of 45° and 55° relative to the shaft axis. Meanwhile, the sonic sensors on the 3,6MW wind turbine were mounted

at a position of 50°. Thus the constants K_1 and K_2 were interpolated between these two positions. The CFD calibrated constants for the 3.6MW wind turbine at the 50° position were derived as:

$$K_1 = 0.875211, \quad K_2 = 0.92183 \tag{9}$$

7.3 Free Field Verification of Spinner Anemometer Constants

The two constants can be checked by measurements of wind speed and wind direction from a free mast during stand still and measurements during yawing of the wind turbine. In case no CFD calibration has been made the free field measurements can be considered as a free field calibration.

Data from the period 11-13 July 2007 have been compared with respect to yaw error. In this period yaw error with a range of about 50° during operation was observed during operation, see figure 48. The comparison shows that the yaw error when measured with mast 3 (mast 3 is directly west of stand 3 where the wind turbine is situated) is only 0,803 of the yaw error when measured with the spinner anemometer, but with an offset of -10°.

Data from March 2007 to April 2008 from the spinner anemometer and the meteorology mast (the meteorology mast is situated on the row of wind turbines south of stand 5) have been used to compare wind speeds, see figure 49. The data were filtered for a 90° sector from the west and for rotational speeds below 4rpm, which means that the rotor is idling. Figure 49 shows a gain factor of 0,989, which is close to 1. Interestingly, the figure also shows data for negative wind speed values of the spinner anemometer, but with a different gain factor of -0,374. The negative wind speed values means that the wind turbine is having wind coming in from the back.

The different gain factors obtained for the yaw error and wind speed comparisons means that the K factors should be adjusted. Meanwhile, this has not been done for the presented results. Therefore, some deviations, especially an over-estimation of the yaw error is present in the data shown in the following chapters.
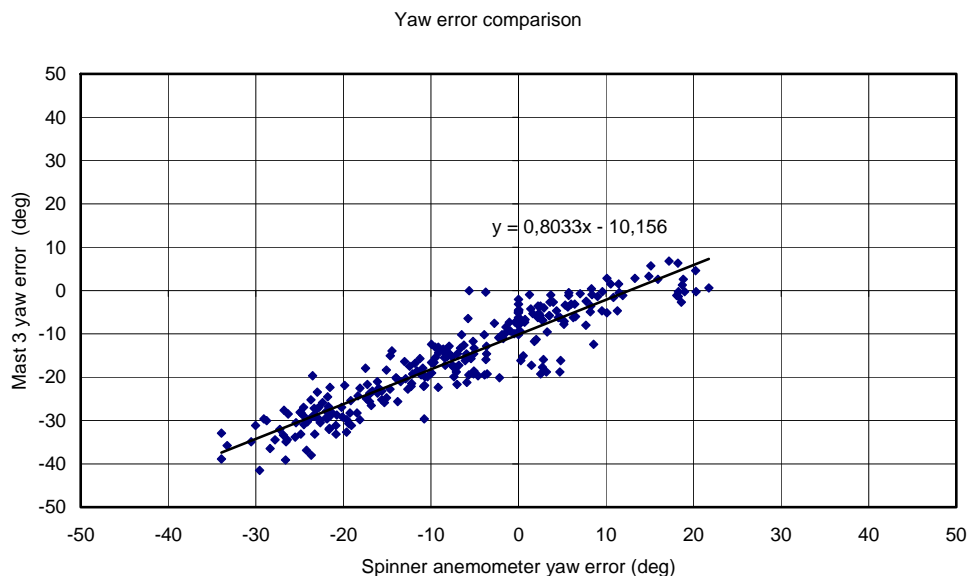
Yaw error comparison

Figure 48 Comparison of yaw error during operation measured by spinner anemometer and by wind vane on mast 3 subtracted yaw direction.
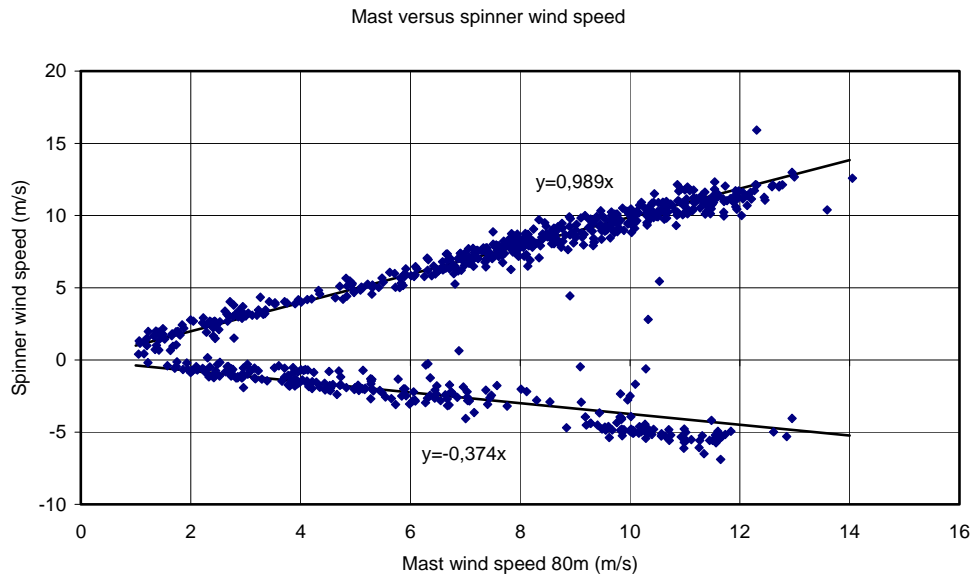
Figure 49 Comparison of wind speeds measured by spinner anemometer and by meteorological mast at 80m height for westerly winds (90°) and rotational speed below 4rpm.

7.4 Measurement Campaign

The spinner anemometer was operated for a period from 14 March 2007 until April 2008. The spinner anemometer worked throughout the period and data were stored together with rotor azimuth measurements on a measurement computer mounted in the hub of the wind turbine. The individual sonic sensors did have down periods, and one sensor gave only a meaningful signal for about half of the period with shorter or longer down time. The reason for down periods was due to weak cable and cable connections, which was known on beforehand from wind tunnel measurements and model field measurements. Only data where all sonic sensors worked satisfactorily have been selected for statistical analysis. The 3.6MW wind turbine is a prototype wind turbine. This means that many tests and activities were performed on the wind turbine in the measurement period. The wind turbine has been stopped for periods, and in other periods it has been operated in special modes. The result was a database of about 10,000 10min data sets. The data sets consisted of time series of 35Hz sampled data.

7.5 Operational Statistics of Spinner Anemometer

From the database statistics was derived with the use of the spinner anemometer algorithm. The analysis gave statistics of 10min average wind speeds, yaw errors and flow inclination angles. The yaw error of the wind turbine is plotted in Figure 50 as 10min average values as function of the 3D measured wind speed. A method of bins analysis (MOB) was performed on the data, and the result is shown with red squares. The flow inclination angle was corrected for a 6° tilt in order to present the flow inclination angle relative to the horizon. The flow inclination angle is shown in figure 51. The presented data are based on the CFD calculations and the K_2 factor was not corrected for the field calibration shown in an earlier chapter.
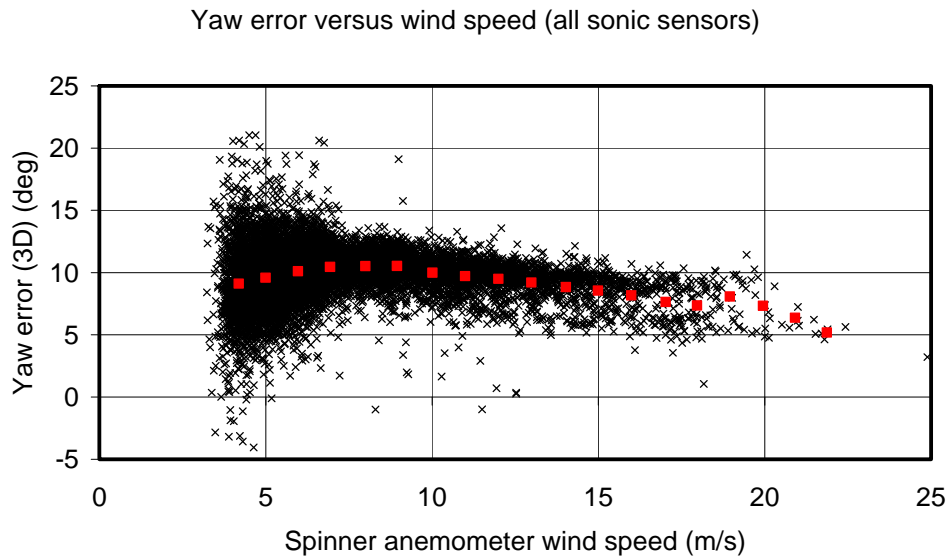
Yaw error versus wind speed (all sonic sensors)

Figure 50 Yaw error as function of 3D measured wind speed (10min averages).

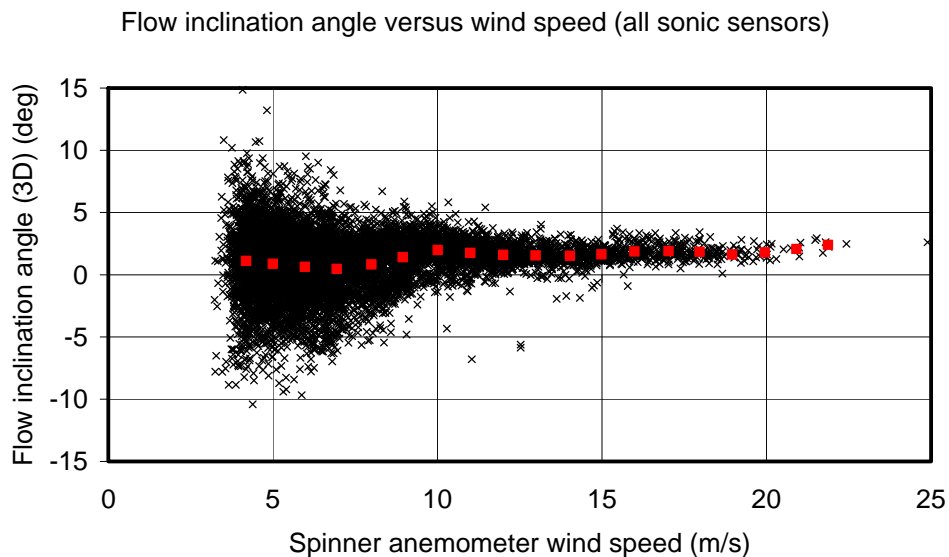Flow inclination angle versus wind speed (all sonic sensors)

Figure 51 Flow inclination angle as function of 3D measured wind speed (10min averages).

The 3D statistics of the yaw error in Figure 50 shows an average yaw error at 4m/s of about 9°, increasing to about 11° at 8m/s and being reduced to about 5° above 20m/s. The flow inclination angle in figure 51 seems to start at 1° at 4m/s, reducing to about 0° at 7m/s, then increasing to about 2° at 10m/s and increasing to about 3° above 20m/s. The flow inclination angle was expected to be 0° in average at all wind speeds due to the very flat site. The reason for the angle not being equal to 0° may be that the conversion factor K_2 is too high.

7.6 Measurements Based on 1D Conversion Algorithm

The spinner anemometer is normally operated with three 1D sonic sensors. This ensures that instantaneous wind speed, yaw error and flow angle are measured. But the spinner anemometer can be operated with only one 1D sonic sensor. Each sonic sensor rotates and delivers measured wind speeds from all azimuth positions. Over time these wind speeds give comparable values to the average values from the 3D

wind measurement. A single 10min average data set from 9 March 2007 at about 7m/s was chosen for an analysis and comparison of operation with three or one 1D sonic sensors. Sampling rate was 35Hz giving 21000 samples per 10min. For the 3D and single 1D sensor measurements a moving average of 1min was used. Figure 52 shows wind speed time traces of instantaneous 3D measurements, 1min moving averaged 3D measurements, and 1min averaged 1D measurements. Figure 53 shows yaw error time traces and figure 54 shows flow inclination angle time traces. The yaw error is defined as the wind speed minus the yaw direction.
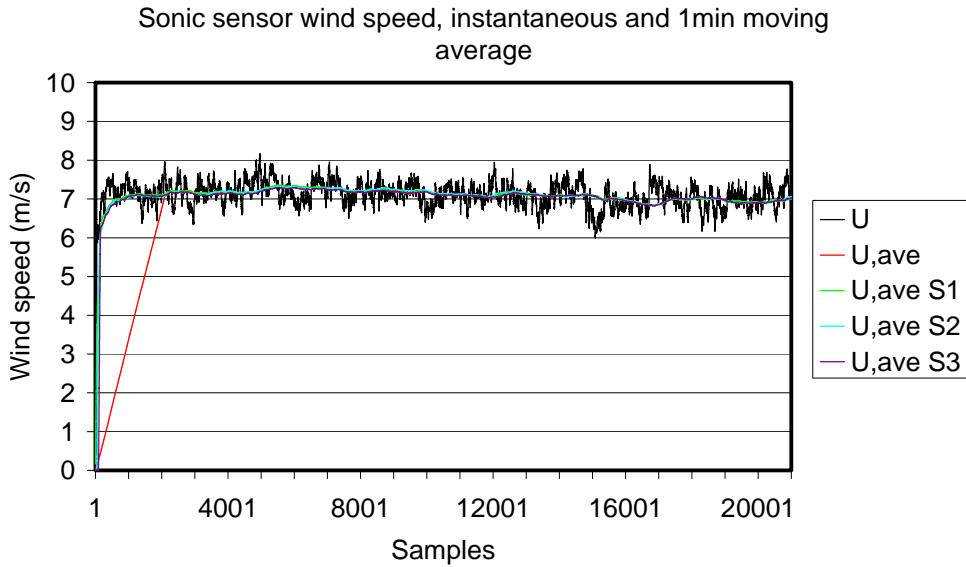

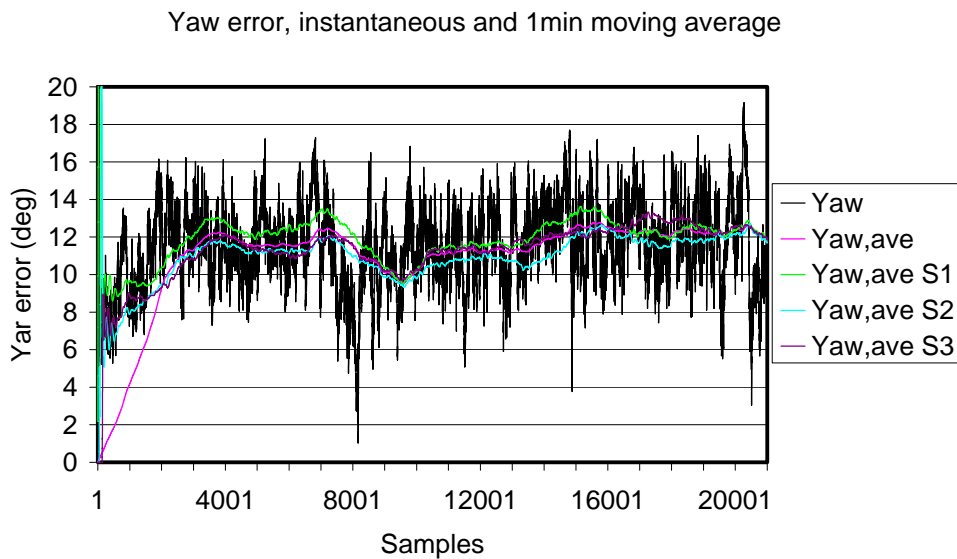*Figure 52 Wind speed time traces of instantaneous and averaged data*

Figure 53 Yaw error time traces of instantaneous and averaged data

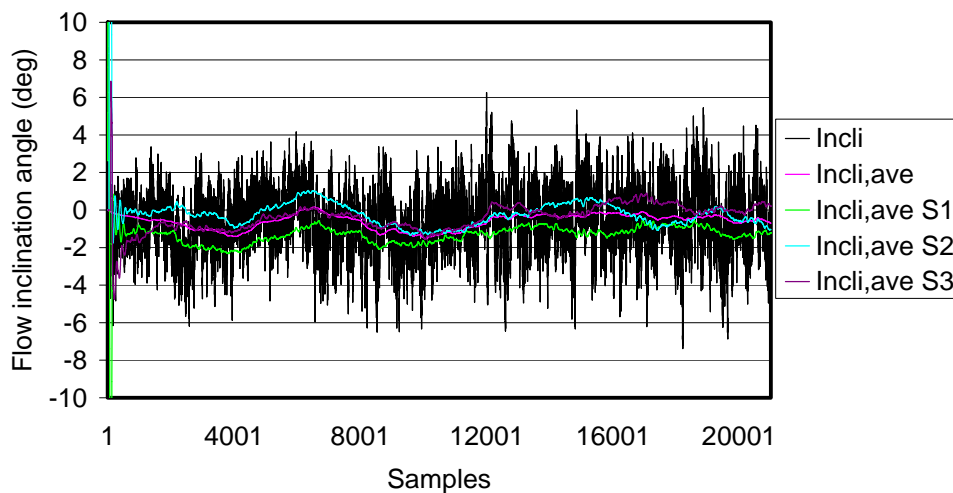Flow inclination angle, instantaneous and 1min moving average

Figure 54 Flow inclination angle time traces of instantaneous and averaged data

The wind flow time traces in figure 52 to 54 show both instantaneous and 1min averaged values. The average values from the 3D measurement uses a 1min moving average window. This is why the averaged value has a gradual slope from the zero starting value to the correct level in the beginning of the graphs in figure 52 and 53. Afterwards, the moving average corresponds very well to the instantaneous values. The average values of the measurements with each sensor were made with a totally different averaging process. This process ensures that the average value is quite close to the correct level value already after one revolution. The comparison of the 3D and 1D average values in the figures shows that the 3D values lye nicely within the variations of the 1D values, which was expected. The angle band of the three 1D values covers 2-3°, and actually there seem to be a systematic difference between them. This is not necessary the case when considering a longer time interval.

Figure 55 and 56 shows statistics determined by the use of only one sensor. Comparisons to figure 50 and 51 shows that there do not seem to be any difference between measurement statistics determined from the use of all three sensors or only one sensor.
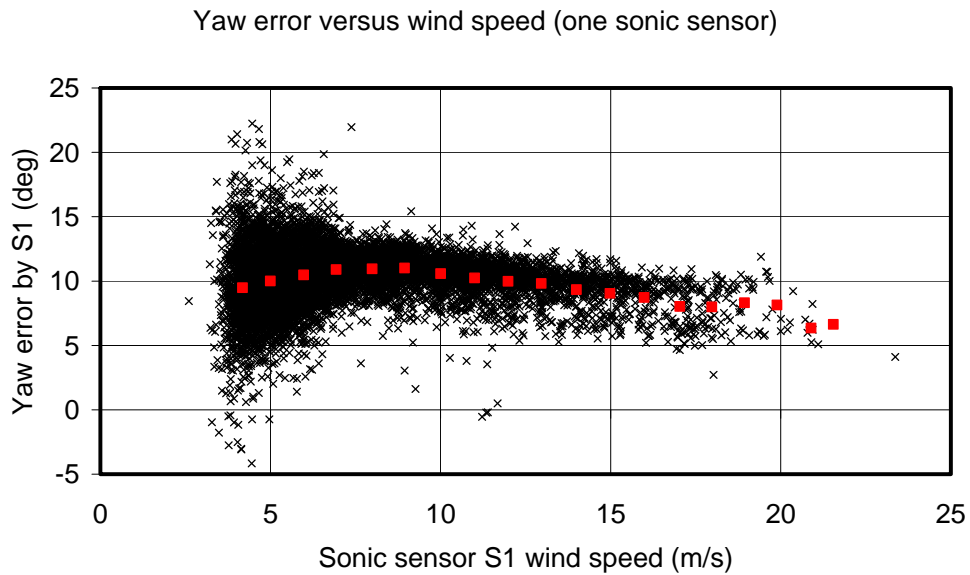
Yaw error versus wind speed (one sonic sensor)

Figure 55 Yaw error as function of 1D measured wind speeds (10min averages).

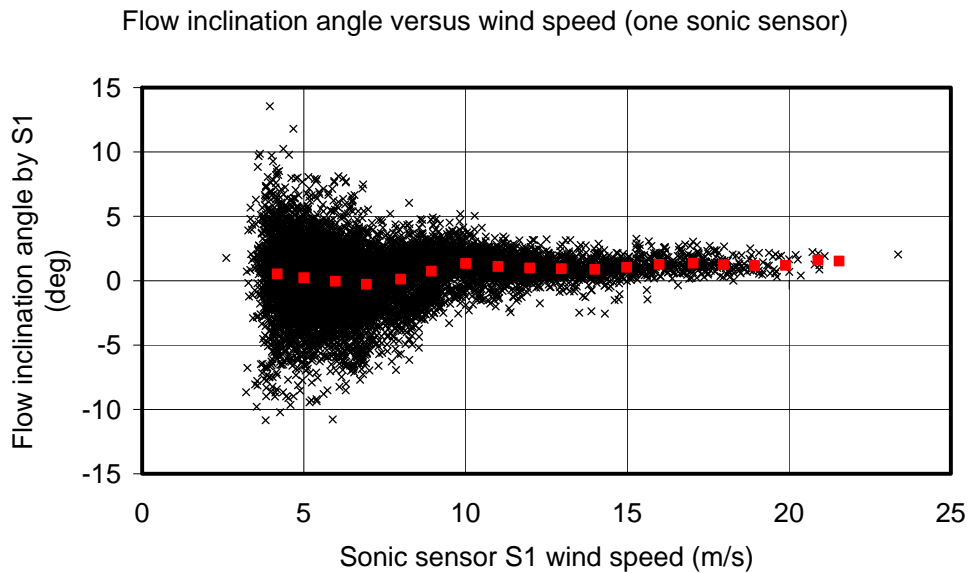Flow inclination angle versus wind speed (one sonic sensor)

Figure 56 Flow inclination angle as function of 1D measured wind speeds (10min averages).

7.7 Determination of Rotor Induced Wind Speeds at Spinner

During operation the induced wind speed due to the blades on the rotor introduces a speed down of the wind in front of the spinner, and the wind speed measured by the spinner anemometer is therefore not fully representing the free wind. This speed down can be determined from measurements during normal operation and be compared with measurements while the wind turbine is idling.

Figure 57 shows the relation between mast wind speed measurements (met mast on row of wind turbine south of stand 5) and spinner anemometer during normal operation. The straight line in the graph is the regression line from measurements during idling. The speed down is clearly seen in the whole wind speed range, being a relative maximum of about 15% at 10m/s.
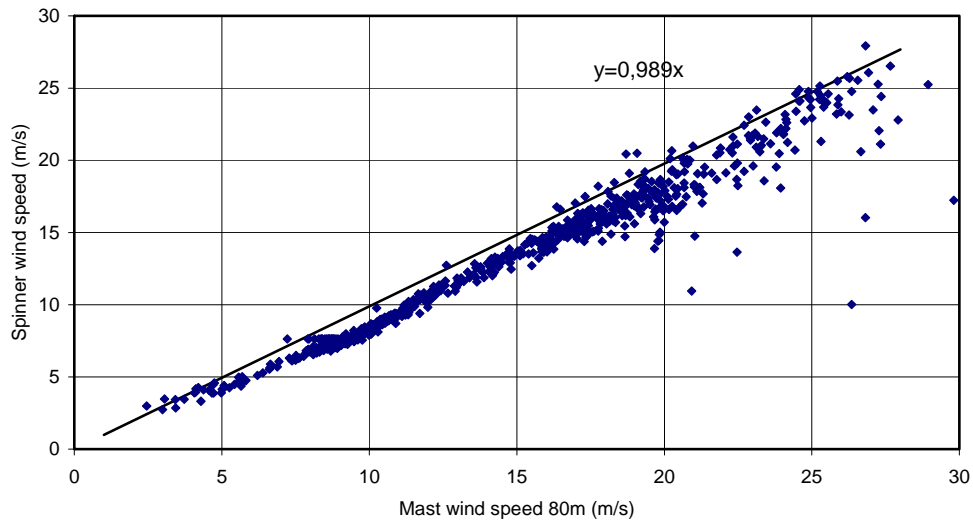
Mast versus spinner wind speed during operation

Figure 57 Rotor induced wind speeds during normal operation. The straight line is from linear regression of data during idling of the wind turbine.

8 Power Versus Measured Yaw Error

Investigations of power performance at skew airflow [12] indicate that the power output of a wind turbine is reduced with a $\cos^2$-function of the yaw error, see figure 58. This means a reduction of power of 1%, 3%, 7% and 22% for average yaw errors of 5º, 10º, 15º and 20º, respectively. Typically, the yaw error is measured to have a spreading with 10min averages of about 5º as shown in figure 59 and 60. This spreading of yaw error increases the power reduction because of the un-linearity of the $\cos^2$ function.

This means that there is a significant gain in power to be achieved if the yawing is optimised. A yaw error of about 10º was measured with the spinner anemometer on the 3,6MW wind turbine, as shown in figure 50. The comparison of yaw error with wind vane in figure 48 showed a gain value of 0.80 which indicates that the yaw error is about 20% over-estimated. If we now assume an average yaw error of 8º and a standard deviation of 2º then the power losses compared to axial flow from Figure 58 shows a power loss of 3.8%. If the yawing were improved to have a yawing error of an average of 0º and a standard deviation of 2º then the losses would be reduced to 1,9%. This would indicate that an increase in power of 1.9% is possible by optimizing the yaw error.

Power versus yaw
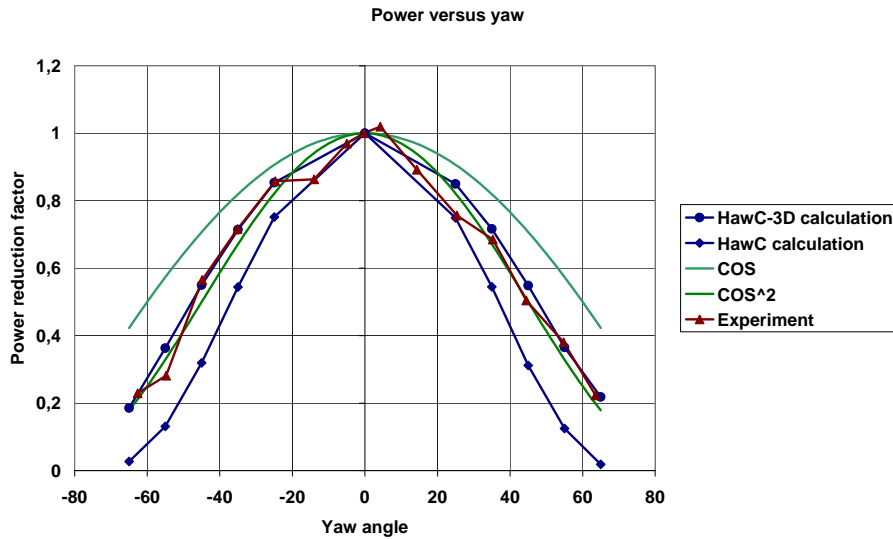
Figure 58   Power losses as function of yaw error calculated and measured from [12].

Figure 59 Typical measured yaw error characteristics of a wind turbine in flat terrain
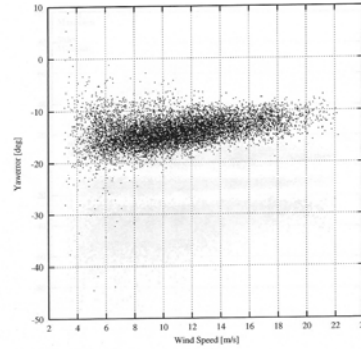
Figure 60 Typical measured yaw error characteristics of a wind turbine in complex terrain

PowerLoss at Tilt Angle 6deg

Figure 61 Estimated power loss for a spreading (std.dev.) of 1° and 5°, respectively. Even with an average yaw error of 0° the tilt angle of 6° will always influence on the power loss.

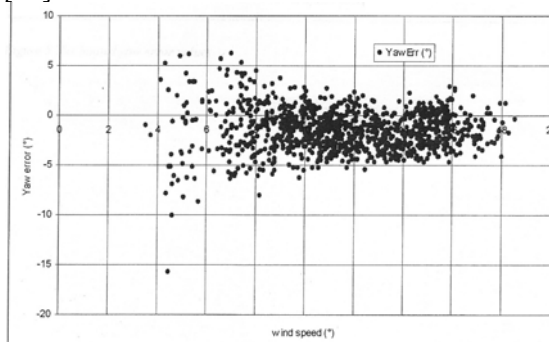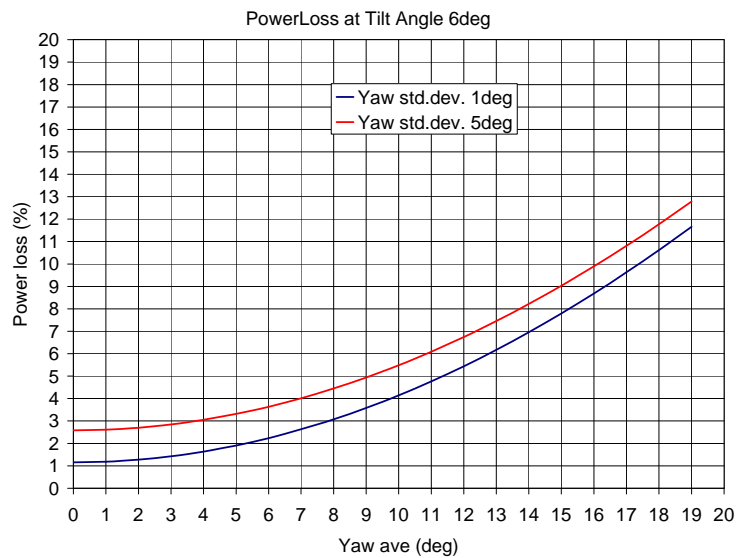The power of the 3,6MW wind turbine was analysed for three days 11-13 July 2007, where some forced yaw errors were found. The results are shown in figure 62 and 63. The figures show that the power from -15º to -5º in yaw error in the mid wind speed range is visibly higher than the power from yaw error beyond -15º. Otherwise, the figures do not show significant differences. This is because differences as small as 1% are difficult to determine with the high spreading in the data, and because the time series data are too limited at the different yaw error angles.
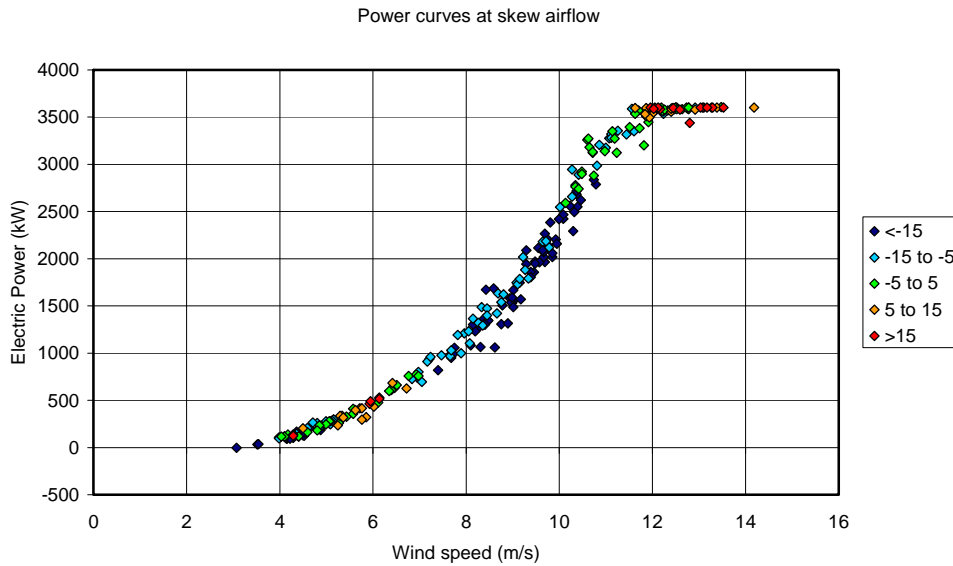

Figure 62 Compared power of 3.6MW wind turbine for measured yaw errors of the spinner anemometer.
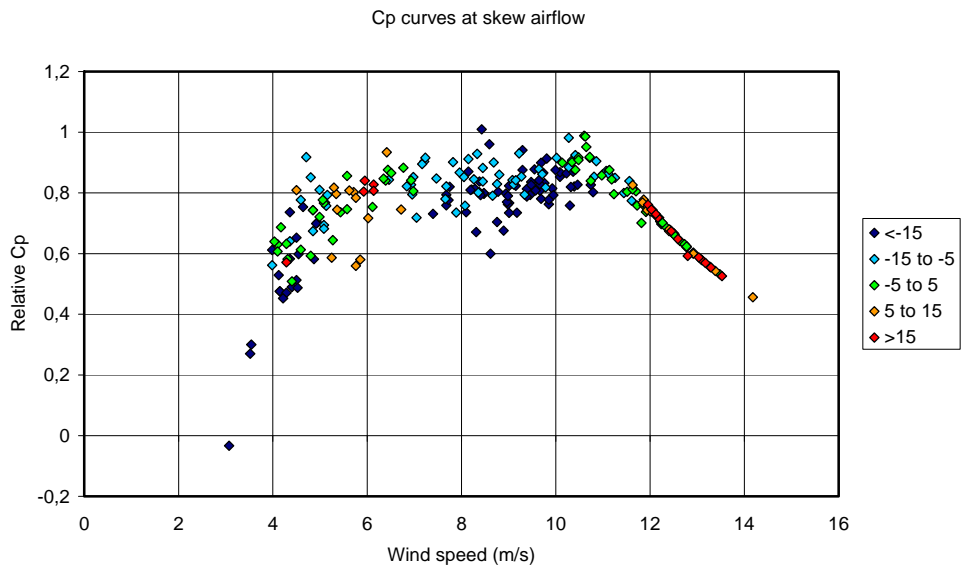

Figure 63 Compared relative Cp of 3.6MW wind turbine for measured yaw errors of the spinner anemometer

9 Summary and conclusions

A new wind measurement concept, a spinner anemometer, has been tested. Testing has been performed by wind tunnel testing, field testing of a model spinner anemometer and comparison to a standard sonic anemometer, and field testing on a full-scale 3,6MW wind turbine.

A prototype spinner anemometer was developed from a standard scientific sonic anemometer with specially designed 1D sonic sensors. The sonic sensors were made in two configurations, one with classic sensor heads and one with small sensor heads.

A model spinner anemometer was tested in wind tunnel with the two sensor head configurations. The tests showed that the sonic sensors responded with a high influence factor on yaw errors, and that the sensors responded with sinusoidal behaviour to rotation of the spinner. The tests also revealed a significant "sensor head flow distortion effect" from the classic sensor heads.

A full CFD analysis of the model spinner anemometer was made. The results showed that the calculations were almost insensitive to rotation and to wind speeds. For all flow or yaw angles up to 60° the azimuth variation was a pure sinus. At 80° yaw there was a significant deviation from the cosine form. The shape of the responses of the sonic sensors to a flow or yaw angle was found to be described with a simple function that over one revolution decreases the average value with a cosine to the flow angle and increases the amplitude with a sine to the flow angle. The function can be described for all three sonic sensors with only two spinner anemometer constants K_1 and K_2, and from the equations, the wind speed, the flow angle to the rotor axis and the azimuth position on the spinner can be determined. This relation can easily be used in a conversion algorithm for the spinner anemometer.

Field measurements were made with the model spinner anemometer and the sonic sensors with small sensor heads. The conversion algorithm was used with the K factors from the CFD analysis with no sensor head corrections applied. An internal calibration of the sensor heads were made, in which sensor 2 and 3 were linearly regressed to sensor 1. The spinner anemometer measurements were compared to measurements from a standard 3D sonic anemometer. The results showed time traces of the two instruments that were very similar. Over a period of three hours, the average wind speed values of the spinner anemometer were 2.5% higher than the sonic anemometer, and the standard deviation values were 4.5% lower. A 1D algorithm, in which only the output of one sensor was moving averaged over about 1 minute, was implemented and it was shown that the averaged results of each sensor compared very well with the averaged 3D conversion algorithm results.

The prototype spinner anemometer with the small sensor heads was mounted on a 3.6MW prototype wind turbine and has been operated for about one year. The conversion algorithm was based on K factors determined from CFD analysis of the spinner and nacelle. The analysis included an internal calibration of the sonic sensors, which indicated that there were significant in-accuracies in geometry and mounting. The internal calibration seems to correct all in-accuracies in geometry and mounting well. A filtered database of the measurements during this period was analysed. Comparisons were made of measurements using all three sonic sensors

(3D) with measurements using only one sonic sensor (1D). The analysis showed that the 1min averaged wind components with 1D measurement also in this case compared quite well with the 3D measurements. Statistics of the yaw error and flow inclination angle was determined from the filtered database. The average yaw error at 4m/s was about 9°, increasing to about 11° at 8m/s and decreasing to about 5° above 20m/s. The flow inclination angle seems to start at 1° at 4m/s, reducing to about 0° at 7m/s, then increasing to about 2° at 10m/s and increasing to about 3° above 20m/s. The spinner anemometer measurements were correlated with wind speed and wind direction from a meteorology mast. A test case of three days of data, where the wind turbine operated while the wind varied to both sides, was compared with yaw error measurements with use of the mast. The results showed that the gain factor of the yaw error was only 0.80, which indicates that the yaw error measurements were overestimated with the use of the K factors from the CFD analysis (the K_2 factor should be corrected to account for this difference). The wind speed at the free mast ahead of the wind turbine was compared to the wind speed measured by the spinner anemometer while the wind turbine was yawing while idling or stopped. The results showed that average wind speeds compared well within about 1% (the gain factor was 0.989). This indicates that the K_1 factor was well estimated from the CFD analysis. The results also showed that the wind speed was determined while the wind turbine was having the wind coming from behind. In this case the wind speed is negative, but the gain factor was reduced to less than the half (-0.37) compared to wind coming from the front. The power of the 3,6MW wind turbine was analysed for varying yaw error for a three day data set. Though the yaw error varied with more than ±20° during the period it was not possible to verify an expected $\cos^2$ variation of power with yaw angle. The reason is that there was not sufficient data at all relevant wind speeds at the different yaw angles.

10 References

1. IEC61400-12-2 Ed.1 WIND TURBINES - Part 12-2: Power performance of electricity producing wind turbines based on nacelle anemometry (Committee Draft 88/325/CD 2008)

2. Jeppe Johansen, graph provided by Jeppe Johansen, AED Risø DTU, through private communication

3. Pedersen TF, Sørensen NN, Enevoldsen P, Egedal P, "Spinner Anemometry - an innovative wind measurement concept", *Proc. EWEC 2007 Milan 7--10 May 2007*

4. Pedersen TF, Sørensen N, Enevoldsen P, "Aerodynamics and Characteristics of a Spinner Anemometer", International conference: The science of making torque from wind, Lyngby (DK), 28-31 Aug 2007*J. Phys.: Conf. Ser.* 75 012018 (9pp)

5. Sørensen NN, Pedersen TF, "CFD computation around wind turbine spinner and nacelle", Risø-I-2579(EN), June 2007, (available on request)

6. Pedersen TF, L Vita, Sørensen NN, Enevoldsen, "Operational Experiences with a Spinner Anemometer on a MW Size Wind Turbine", *Proc. EWEC 2008 Bruxelles 31 March-3 April 2008*

7. Thurtell GW, Tanner CB, Wesely ML, 1970, "Three-Dimensional Pressure-Sphere Anemometer", Journal of Applied Meteorology Volume 9 pp379-385

8. Wesely ML, Tanner CB, 1972 "An Improved Pressure-Sphere Anemometer", Boundary Layer Meteorology pp275-283

9. Cuerva A, Snaz-Andrés A, Franschini S, Eecen P, Busche P, Pedersen TF, Mouzakis F, "ACCUWIND, Accurate Wind Measurements in Wind Energy, Task 2, Improve the Accuracy of Sonic Anemometers", EU-FP6 project report, June 2006

10. Wieser A, Fiedler F, Corsmeier U (2001), "The influence of the sensor design on wind measurements with sonic anemometer systems", Journal of Atmospheric and Oceanic Technology 18: 1585-1608, Boston (USA)

11. Tammelin B, Heimo A, Leroy M, "Ice-free sensors - The EUMETNET SWS II project", Finnish Meteorological Institute, Helsinki

12. Pedersen TF, Gjerding S, Ingham P, Enevoldsen P, Hansen JK, Jørgensen HK, "Wind Turbine Power Performance Verification in Complex Terrain and Wind Farms", Risø-R-1330(EN)

www.risoe.dtu.dk